AD-A194 888 DAMAGE INITIATION IN THE SHORT BEAM SHEAR TEST OF COMPOSITE MATERIALS USI (U) AIR FORCE INST OF TECH WRIGHT-PATTERSON AFB OH SCHOOL OF ENGI... D T DUPONT

1/2

UNCLASSIFIED JUN 88 AFIT/GAE/AA/87D-5 F/G 11/4 NL

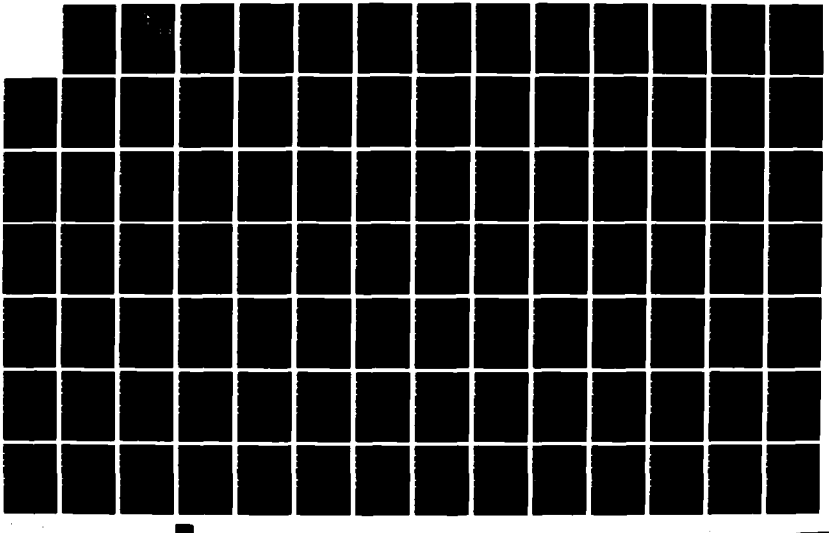

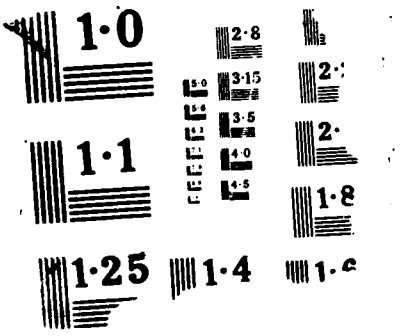
1·0
1·1
1·25
1·4
2·8
3·15
3·5
4·0
4·5
2·
1·8

DAMAGE INITIATION IN THE SHORT BEAM SHEAR TEST OF COMPOSITE MATERIALS USING STIFFNESS REDUCTION

THESIS

Dean Thomas Dupont
Captain, USAF

AFIT/GAE/AA/87D-5

DEPARTMENT OF THE AIR FORCE
AIR UNIVERSITY
AIR FORCE INSTITUTE OF TECHNOLOGY
Wright-Patterson Air Force Base, Ohio

AFIT/GAE/AA/87D-5

DAMAGE INITIATION IN THE SHORT BEAM SHEAR TEST OF COMPOSITE MATERIALS USING STIFFNESS REDUCTION

THESIS

Dean Thomas Dupont
Captain, USAF

AFIT/GAE/AA/87D-5

AFIT/GAE/AA/87D-5

DAMAGE INITIATION IN THE SHORT BEAM SHEAR TEST OF COMPOSITE MATERIALS USING STIFFNESS REDUCTION

THESIS

Presented to the Faculty of the School of Engineering
of the Air Force Institute of Technology
Air University
In Partial Fulfillment of the
Requirements for the Degree of
Master of Science in Aeronautical Engineering

Dean Thomas Dupont, B.S.
Captain, USAF

June 1988

Preface

The purpose of this study was to examine the feasibility of modeling damage initiation in composite materials using finite elements. Composites have become an important part of aircraft design. The ability to model and predict damage initiation will help in the design as well as the failure tolerance analysis of structures comprised of composite materials. An existing finite element code, NOSAPM, was modified to include a failure criteria and stiffness reduction techniques. Along with the headaches of changing a complicated code such as NOSAPM were the problems of converting the mounds of generated data into something useful. The post-processing routines originally written for NOSAPM are either extinct or well hidden within the bowels of the Wright-Patterson AFB computer network.

Amidst the problems and false starts associated with this project are people to whom I am extremely grateful. First and foremost, my thanks go to Mr. Ted Feke, my sponsor, who provided the resources and the motivation for this study. I also would not have completed this work without the patience, guidance, understanding, and insight of my advisor, Major Paul Copp. Finally, I wish to thank my beautiful wife and partner, Tina, who has taught me new meanings of the words love and patience.

Table of Contents

	Page
Preface	ii
List of Figures	iv
Abstract	vi
I. Introduction	1
II. Background	4
III. Development of Solution	16
Configuration Model	18
Finite Element Model	22
Damage Criteria	25
Stiffness Reduction	30
Stress Field	32
IV. Results and Discussion	35
Shear Test Stress Fields	35
Damage Criteria in NOSAPM	45
Stiffness Reduction in NOSAPM	48
V. Conclusions and Recommendations	74
Appendix A: Using NOSAPM for Stiffness Reduction	76
Appendix B: Subroutine DAMAGE	84
Bibliography	89
Vita	92

List of Figures

Figure		Page
1.	Short Beam Shear Test Configuration (Three Point Bend Test).....	17
2.	Fiber Orientation Directions (a) zero degrees,(b) ninety degrees.....	21
3.	Finite Element Model Mesh Geometry.....	26
4.	Stresses Analyzed for Damage Criteria.....	34
5.	Section of Beam Stress Field Plotted.....	36
6.	P = 20 lb, Normal Stress Ninety Degree Fiber Orientation.....	38
7.	P = 20 lb, Normal Stress Zero Degree Fiber Orientation.....	39
8.	P = 20 lb, Shear Stress Ninety Degree Fiber Orientation.....	40
9.	P = 20 lb, Shear Stress Zero Degree Fiber Orientation.....	41
10.	P = 20 lb, Bending Stress Ninety Degree Fiber Orientation.....	43
11.	P = 20 lb, Bending Stress Zero Degree Fiber Orientation.....	44
12.	P = 20 lb, Ninety Degree Fiber Orientation Eq (9), Tsai-Hill.....	46
13.	P = 20 lb, Zero Degree Fiber Orientation Eq (9), Tsai-Hill.....	47
14.	Single Element Compression Check Configuration.....	51
15.	Eq (9), Tsai-Hill, 0% Stiffness Reduction Constant Load, P = 3 lb.....	55

16. Eq (9), Tsai-Hill, 50% Stiffness Reduction Constant Load, P = 3 lb..... 56

17. Eq (9), Tsai-Hill, 95% Stiffness Reduction Constant Load, P = 3 lb..... 57

18. Normal Stress, 0% Stiffness Reduction Constant Load, P = 3 lb..... 59

19. Normal Stress, 50% Stiffness Reduction Constant Load, P = 3 lb..... 60

20. Normal Stress, 95% Stiffness Reduction Constant Load, P = 3 lb..... 61

21. Shear Stress, 0% Stiffness Reduction Constant Load, P = 3 lb..... 62

22. Shear Stress, 50% Stiffness Reduction Constant Load, P = 3 lb..... 63

23. Shear Stress, 95% Stiffness Reduction Constant Load, P = 3 lb..... 64

24. Bending Stress, 0% Stiffness Reduction Constant Load, P = 3 lb..... 66

25. Bending Stress, 50% Stiffness Reduction Constant Load, P = 3 lb..... 67

26. Bending Stress, 95% Stiffness Reduction Constant Load, P = 3 lb..... 68

27. Bending Stress, 95% Stiffness Reduction Ramp Load..... 71

28. Normal Stress, 95% Stiffness Reduction Ramp Load..... 72

29. Shear Stress, 95% Stiffness Reduction Ramp Load..... 73

30. Changes to NOSAPM Data..... 77

31. Job Control Listing for NOSAPM..... 81

32. Source Listing of Subroutine DAMAGE..... 87

Abstract

The purpose of this study was to analyze damage initiation in the short beam shear test for composite materials. This thesis proposes a means of predicting damage initiation in a composite beam using finite element techniques and a continuum mechanics failure criteria. The first objective was to accurately determine the stress field. The second objective was to employ a damage criteria based on the elemental stress field. The final objective was to evaluate the effectiveness of using an elemental stiffness reduction to study damage initiation and progression. The finite element code used was NOSAPM.

The complex stress fields associated with this problem were accurately obtained with the exception of the shear stresses. The high shear gradients required the use of a very fine mesh which was not possible with the computer resources available. The Tsai-Hill failure criteria was successfully incorporated into NOSAPM. Also, an elemental stiffness routine was derived and verified with a single element compression case. With the beam test model, the stiffness reduction technique did not dramatically affect

the material with fibers oriented ninety degrees. However, the zero degree fiber orientation case resulted in stress contour changes which suggested a spreading of the load through an element. This spreading only occurred with a stiffness reduction greater than ninety-five percent. At high loads and stiffness reductions, the model breaks down as the numerical solutions result in element instabilities.

The most significant recommendations are to refine the mesh using a two dimensional code and to reduce the stiffness only in the area best representing the failure mode. Also, load shifting should be investigated to prevent the elemental instabilities. Finally, a study using an indentor model instead of a point load should be accomplished.

Damage Initiation in the Short Beam Shear Test of Composite Materials using Stiffness Reduction

I. Introduction

An important topic in the study of the mechanics of materials is the characterization of damage. The ability to predict damage enables an engineer to account for it and to make the required design changes as appropriate. Conventional materials such as steels and metal alloys have fairly well established damage behaviors. Composite materials, however, often do not fail in the same mode as their metal counterparts. With the increased use of composites in aircraft design, better techniques are needed to evaluate and predict damage to such composite materials as graphite/epoxy and the more exotic metal matrix materials. This thesis is an attempt to understand one aspect of damage modeling, the initiation of damage caused by a bending load.

Material properties are determined by testing. Pure tension and compression tests have been used predominantly

due to the simplicity of specimen loading and geometry. These tests provide an understanding of failure by reducing the number of variables considered. However, biaxial tests like the short beam shear test provide a more complex stress field and require more insight into the modes of material damage. This short beam test is now being scrutinized to determine its effectiveness as a means of measuring interlaminar shear strength. The complex stress field of the test has produced local failures that occur prior to the expected shear delaminations thus casting suspicion on test results. Comprehensive modeling of damage initiation and progression is essential in developing an understanding of this phenomena.

In order to make an assessment of composite damage and how to model it one must first understand how it originates. To date, test observations are inconclusive as catastrophic failure occurs too rapidly to allow identification and measurement of local and global damage. Also, the microscopic details of the physics of composite damage have not been fully explained or modeled. This thesis proposes a means of predicting damage initiation in a composite beam using finite element techniques and a continuum mechanics failure criteria. The first objective is to accurately determine the stress field for the short beam shear test of a compos-

ite beam. A convergence study of the required mesh will be conducted using the finite element code NOSAPM. The second objective is to employ a continuum mechanics damage criteria that predicts damage based upon the elemental stress field. The third objective is to determine the effectiveness of using stiffness reduction to study damage initiation and progression. Stiffness reduction methods have been employed successfully in simple stress fields. It is of fundamental interest to determine if these methods can also be successfully applied to complex stress fields to accurately characterize the experimentally observed local and global failure modes. The results of this thesis will serve as a basis to determine the most fruitful approach that should be pursued by follow-on efforts to characterize damage in composite materials.

II. Background

The question of how to model damage in composite materials is not a new one. Various methods have been employed to try to describe the phenomena of material failure. To begin with, failure must first be defined. The point when a load exceeds the capacity of a structure to elastically support it, normally called yielding, is the most widely applied failure criteria. However, for a complex loading a more convenient measure would be a relation of some failure criteria to the entire stress field of the structure. This stress field could be most easily defined by using simple beam theory. But, beam theory breaks down with large displacements and also fails to account for localized loading effects. The strain-displacement and stress-strain relationships of finite element techniques, however, do provide a way to overcome these beam theory limitations. Of course, finite elements do depend significantly on the modeling of the structure and the types of elements used.

Alternatively, one can solve the elasticity contact problem for the complex stress fields produced by a rigid indenter. Such a mixed boundary value problem requires the application of integral transforms. While these techniques

may be more exact, integral transform solutions for multi-layered structures can not be obtained in closed form thus prompting one to use finite elements. Regardless, all numerical techniques must be validated by physical testing, if possible, to determine accuracies and limitations of the modeling.

Damage must be defined using some criteria. Exceeding this criteria indicates damage will occur. As with conventional materials, there exist many theories to define damage in composite materials. The criteria used for this research is based upon the longitudinal, transverse, and shear strengths of the material. It was chosen because it utilizes the three dimensional state of stress throughout the body. For conventional materials this strength is best described by yield criteria such as the Tresca (Maximum Shear Stress) and Von Mises (Distortional Energy) criteria (10:134,139). By using the element's stress fields with a combination of material strengths one obtains an indication of potential failure.

Methods to determine the strength of a composite material are shown by both Jones (8:71,83) and Tsai (17:277,325). Modern theories include the maximum stress theory, the maximum strain theory, the Tsai-Wu tensor theory, and the Tsai-Hill theory. Each of these theories have strengths and

weaknesses, so application of any must be carefully considered. A brief look at each of these theories is necessary to establish the one best suited for this research.

According to Jones, the maximum stress theory requires that the stresses in principal material directions be less than material strengths in those directions (8:72). Thus,

$$\begin{aligned} X_c < \sigma_1 < X_t \\ Y_c < \sigma_2 < Y_t \\ Z_c < \sigma_3 < Z_t \\ |\tau_{12}| < S \end{aligned} \tag{1}$$

where X, Y, and Z indicate material strengths in the respective directions, S is the shear strength, sigma is the stress in the material principal directions, and the subscripts "t" and "c" represent tension and compression, respectively. In a similar manner the maximum strain theory compares the strains in the principal material directions with the maximum allowable strains in those directions. However, these theories do not take into account any combined effects of the complex stress fields.

Wu (21:361-400) published a comparison of the different failure criteria as they pertain to anisotropic materials. He contrasts the use of the maximum stress and strain crite-

ria with anisotropic versus isotropic materials. Wu (21:361) noted that replacing the stress invariants with deviatoric invariants is not possible since hydrostatic and deviatoric yielding has not yet been proven to be independent. Also, as shown by Jones above, material parameters must be in each of the principal directions and invariant to transformations.

A more complex strength criterion was proposed by Tsai and Wu to take into account stress interactions and to be invariant in material transformations (18:58-80). This technique uses two strength tensors in a scalar function to represent a failure surface. This function

$$f(\sigma_k) = F_i\sigma_i + F_{ij}\sigma_i\sigma_j = 1 \qquad (2)$$

contains twenty-seven terms in its expanded form with i,j,k = 1,2,...,6. The coefficients of the resulting stress polynomials are functions of the material strength characteristics, usually determined experimentally (17:280-287). The Tsai-Wu criteria has favorable properties such as built in invariance, ease of transformation, and the ability to show a variety of stress interactions common in a complex field. But, this criteria does require a greater knowledge of material properties and can become somewhat unwieldy.

The final strength criteria to be considered was first proposed as a yield criteria for anisotropic materials by Hill (6) and related to composite strengths by Tsai (16). This Tsai-Hill criteria combines the apparent simplicity of maximum strength with some of the favorable properties of Tsai-Wu. Principal stresses and shear stresses are combined in the following form:

$$(G+H)\sigma_1^2+(F+H)\sigma_2^2+(F+G)\sigma_3^2-2H\sigma_1\sigma_2-2G\sigma_1\sigma_3-2F\sigma_2\sigma_3 + 2L\tau_{23}^2+2M\tau_{13}^2+2N\tau_{12}^2=1 \quad (3)$$

The coefficients F,G,H,L,M,and N are functions of the material strengths. These properties are measured experimentally with established tension, compression, and shear tests. When the summation of the combined strength/stress terms exceeds unity failure is predicted to occur. According to Jones (8:79-80), this theory works well with E glass/epoxy composites. The Tsai-Hill criteria also reduces correctly to the well established maxmum octahedral or Von Mises shear stress theory. Tsai-Hill can be regarded as an accurate measure of composite strength for the load cases and material orientations being investigated.

Along with having a strength criteria, one must have a way of analyzing the problem. One method of solving complex

structural problems is with finite elements. "The finite element method is a numerical procedure for solving a continuum mechanics problem with an accuracy acceptable to engineers" (4:1). With the advent of composite materials came the application of finite element methods to these anisotropic materials. While this field continues to grow as the "real world" is modeled more closely, significant achievements have already occurred. Some of these achievements are presented here.

Finite element modeling of composite material structures is getting more sophisticated as people try to use this powerful analysis tool in more applications. Chamis (2), at the NASA Lewis Research Center in Cleveland, Ohio, reported on their current work using finite element techniques to analyze composite structures. The efforts he cites include integrated composite mechanics analysis, simplified composite mechanics for strength, and a 3-D finite element for micromechanics modeling of composites. This work is related closely with damage and damage prediction. Chamis (2:5) refers to a 3-D finite element model "readily adaptable to investigating interfacial disbonds, fiber breaks, voids and even matrix crack effects on the microstress distribution." This "superelement" is not yet adaptable to many finite element routines, but serves as an example of the level of

sophistication obtainable with finite elements.

Other ways of using the finite element method are shown by Ross and associates (11). They use SAPIV, a general purpose code, and a proprietary code named ABAQUS to model interlaminar delamination. Anisotropy is accomplished by varying material properties along the different axes. ABAQUS has an interface element that is placed between brick elements to show interlaminar behavior. Their results indicate only a finite progression of damage since they are modeling an impact event. Delamination is the failure mode they are interested in studying. Only shear stresses at discrete points are shown as the authors believe that shear is the major cause of delamination. Humphreys (7) uses SAPIV to develop a procedure to show damage accumulation in a composite plate during a low velocity impact. He calculates damage by comparing various combinations of stress and strength. When damage is said to occur in his model the failed element is removed from the mesh. Humphreys shows the global effects of this impact occurrence. These effects resemble plate theory.

Damage progression work done by Witt (20) used a two dimensional finite element model of a specimen in pure tension. Failure around a crack was predicted using two different techniques. The first method used a purely elastic

technique to show the stress field after damage defined by the Tsai-Hill criteria. With the second technique, Witt would completely remove the stiffness of a failed element upon damage. While neither method accurately predicted damage growth, they did provide bounds for the actual phenomenon (20:67).

Shivakumar and Elber (12) used the finite element code, GAMNAS, to model an axisymmetric plate under a low velocity impact. By using the crack closure technique, they sought to identify two modes of delamination, peeling and shear sliding. They only used cases equivalent to static deflections and found that shear sliding was the primary mode of delamination growth. The stress fields resulting from these cases are not presented.

Another use of finite elements to show composite damage is by Chamis and Williams (3) to determine interply layer degradation effects. Applying a central load to a simply supported beam, they looked at the effects that a reduced interply (matrix material) stiffness would have on the beam characteristics. They found that in reducing the interply modulus from one million psi to one thousand psi, no noticeable structural changes occur until around the ten thousand psi level. Although not showing damage progression through the beam, they do show some overall characteristics that

could describe a beam damaged in such a way as to have reduced stiffness properties.

Murthy and Chamis (9) used a NASTRAN finite element model of notched and smooth fiber composite Charpy specimens to determine failure modes. They ran both static and dynamic cases. Their results showed that static and dynamic stress contours are almost identical. The quasi-static representation of the dynamic process was the most conservative. While not concentrating on damage progression, they found that for a notched specimen either normal, longitudinal, or shear stress could cause or initiate a failure. They also observed that shear stresses dominated the transient analysis of the notched specimen. For smooth specimens, combined stresses near the load seemed to be the cause of failure with no one stress tending to dominate.

Along with the flexibility of finite element techniques come certain limitations. Notably, approximations in determining displacements leads to further approximations in stress calculations. More exact methods to determine the stress field using numerical techniques or integral transforms do exist. The latter technique allows one to solve the mixed boundary value problem of an indenter acting on the beam surface. These closed form solutions do provide valuable insight with which to compare the finite element

analyses. However, they can become rather cumbersome and can not be readily extended to include damage mechanisms.

Shivakumar, Elber, and Illg (13) use numerical methods to solve for progressive damage in thin circular laminates under static loads. The minimum total potential energy method combined with Von Karman strain-displacement equations gave them the means to calculate loads as well as ply stresses. They used the Tsai-Wu criteria to determine when failure occurs and other combinations of stresses and strengths to evaluate the failure modes. Progression is modeled by eliminating the stiffness in the area of the calculated failure mode. Their analysis concluded that failure started at the bottom-most ply. In terms of damage tolerances, splitting thresholds were lower for larger plates while "first-fiber-failure" thresholds were lower for smaller plates.

Another way of solving the complex mixed boundary continuum mechanics equations is with integral transforms. Copp and Keer (5) analyzed the indentor problem with simply supported composite beams of differing fiber orientations. An extensive parametric study of contact length, layer thickness, beam length, lamina orientation and support conditions was conducted. The resulting stress contours depicted both the local effects of the indentor and the sup-

ports as well as the global beam response. While not using any stiffness reduction scheme for damaged material, Copp and Keer did use the Tsai-Hill criteria to indicate damage patterns in a purely elastic material over various load conditions. The integral transform techniques used did not allow for a progressive increase in loading, but rather controlled loading by specifying the contact length and calculating the corresponding indenter loads. Even with this disparity, the stress contours generated by Copp and Keer will be a valid comparison for any stress field contours generated by this thesis.

Testing provides another method of validation, as well as a means to explore damage progression. Many people have tried to develop empirical damage progression models based on experimental observations. A problem with using test observations is that damage usually occurs quickly. Even if the damage progression can be followed, most instrumentation cannot sort out the complex stress field closely enough to determine which stress or stresses caused the failure. For instance, Whitney and Browning (19) point out some apparent problems with the well established short beam shear test. They claim that shear is not the most dominant of the stresses in the initial stages of the test. The first mode of failure is under the nose of the load applicator. After

initial matrix crushing occurs, shear or other stress combinations then complete the failure process. Their results indicate that the short beam shear test does not give the expected minimum shear strength of the composite material in question.

Clearly, modeling the phenomena of damage initiation requires a failure criteria. Finite elements will be the method of calculating stresses and applying the criteria. Finite elements will also be the means of incorporating stiffness reduction techniques. The stress fields will be compared to those of Copp and Keer (5) for accuracy. Finally, the model will be scrutinized to determine how closely it matches experimental data.

III. Development of Solution

This thesis investigates damage initiation in a beam under a contact load. Damage initiation is defined with respect to exceeding a damage failure criteria. Without actually describing the physics of the damage mechanism such as material separation, fracture, or plastic deformation one can get a good idea of where and how the material would fail by looking at the stress fields during the "failure" process. The phenomenon of damage initiation as it pertains to a contact load on a beam can be shown with a typical three point bend test (Fig. 1). The short beam shear test described by ASTM Standard D2344 is one such test. With this test one derives apparent shear strength properties by loading the specimen to failure and calculating the shear by

$$S_H = \frac{0.75P_B}{bd} \tag{4}$$

where S is the shear strength, P_B is the breaking load or maximum load on the load indicating mechanism for the test, b is the width of the specimen, and d is the thickness of

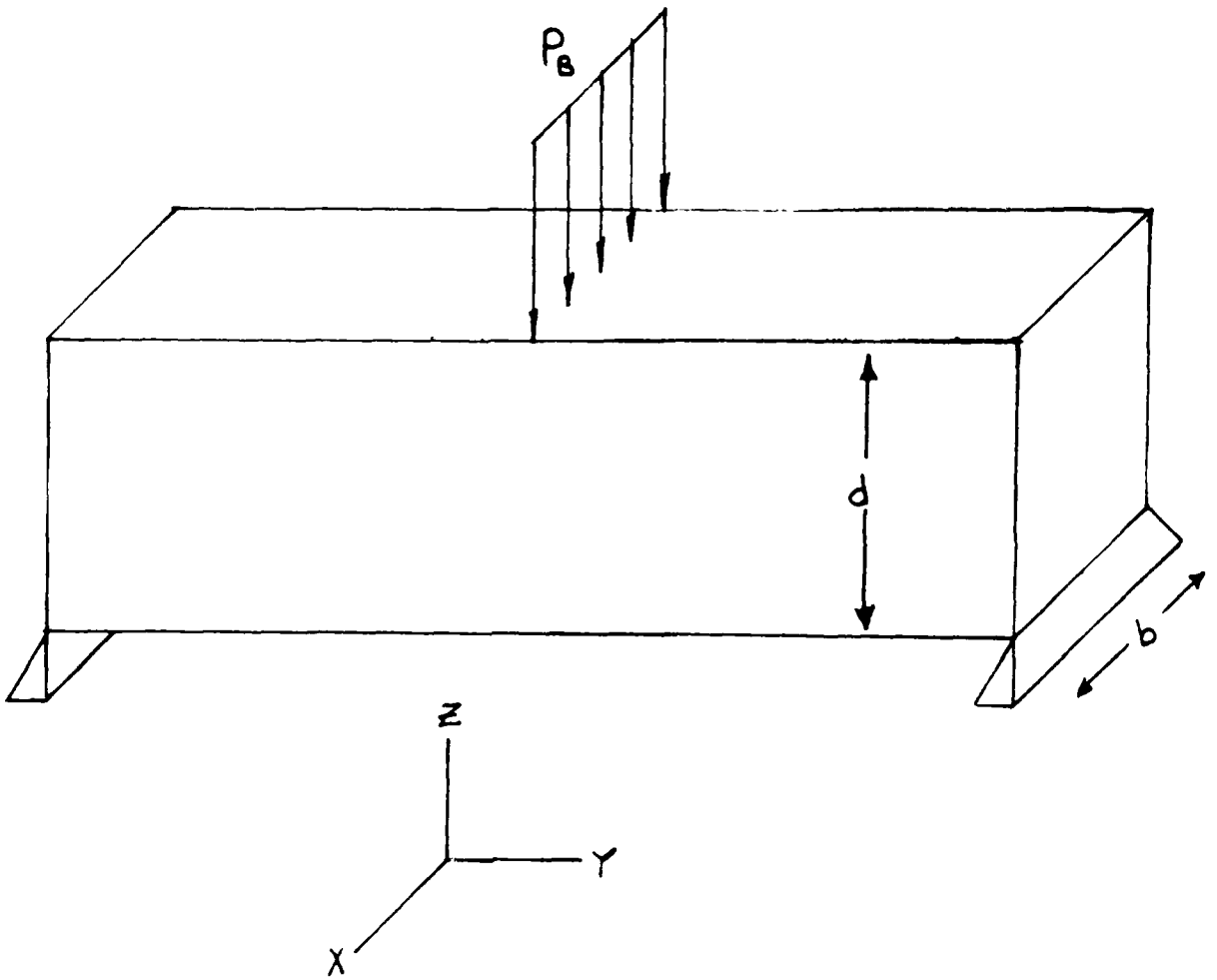

Short Beam Shear Test Configuration

(Three Point Bend Test)

Fig. 1

the specimen (1:56-57). This test is relatively simple, tempting one to use it exclusively in establishing design parameters for the shear strength of composite materials.

But as seen by Copp and Keer (5), the resulting stress field from such a contact problem is quite complex, thus failure is a consequence of more than just pure shear. A need exists to determine the complete state of stress and to translate that stress field into an estimation of damage. Using finite elements and a failure criteria, this thesis analyzes the short beam shear test and the damage initiation characteristics of different fiber orientations in parallel fiber composites.

Configuration Model

The short beam shear test is described in detail by ASTM Standard D2344. A beam is supported at two ends with the load applied in the center (Fig. 1). The load is slowly increased until the beam specimen breaks. The breaking load is defined as the maximum load displayed by the load indicating mechanism used for the test. This failure load is then put into Eq (4) to calculate the apparent shear strength of the specimen. The span length-to-depth ratio limits for test specimens is five (5) for materials rein-

forced with fibers of modulus less than 14.5 million psi and four (4) for fibers of higher modulus. The standard also specifies the sizes of the supports and the load nose. This study is limited to the basic test setup and specimen ratios as noted in the standard. The loading considered is only a point or knife-edge load.

The material for this analysis was a graphite/epoxy type composite with a Young's modulus fiber to resin ratio of about four (4). The material properties used appear in Table 1. The ratio between E_{11} and E_{22} is not quite as large as graphite/epoxy. The fourteen to one ratio usually associated with graphite/epoxy type materials could not be successfully used with NOSAPM. The ratio displayed in Table 1 represents the largest difference in moduli completely checked out with NOSAPM. The fibers are assumed to be parallel with material properties taken as the average over a section. Two orientations of these fibers (Fig. 2) are evaluated to determine their effects on damage initiation. The axis along the fiber is represented by properties denoted by "11" in Table 1. The material axes perpendicular to the fiber are properties "22" and "33". One would

Material Properties

Table 1

Properties	Value
E_{11}	8.0×10^6 psi
E_{22}	1.7×10^6 psi
E_{33}	1.7×10^6 psi
Poisson's Ratio 11	0.30
Poisson's Ratio 22	0.02
Poisson's Ratio 33	0.02
G_{11}	0.8×10^6 psi
G_{22}	0.8×10^6 psi
G_{33}	0.8×10^6 psi

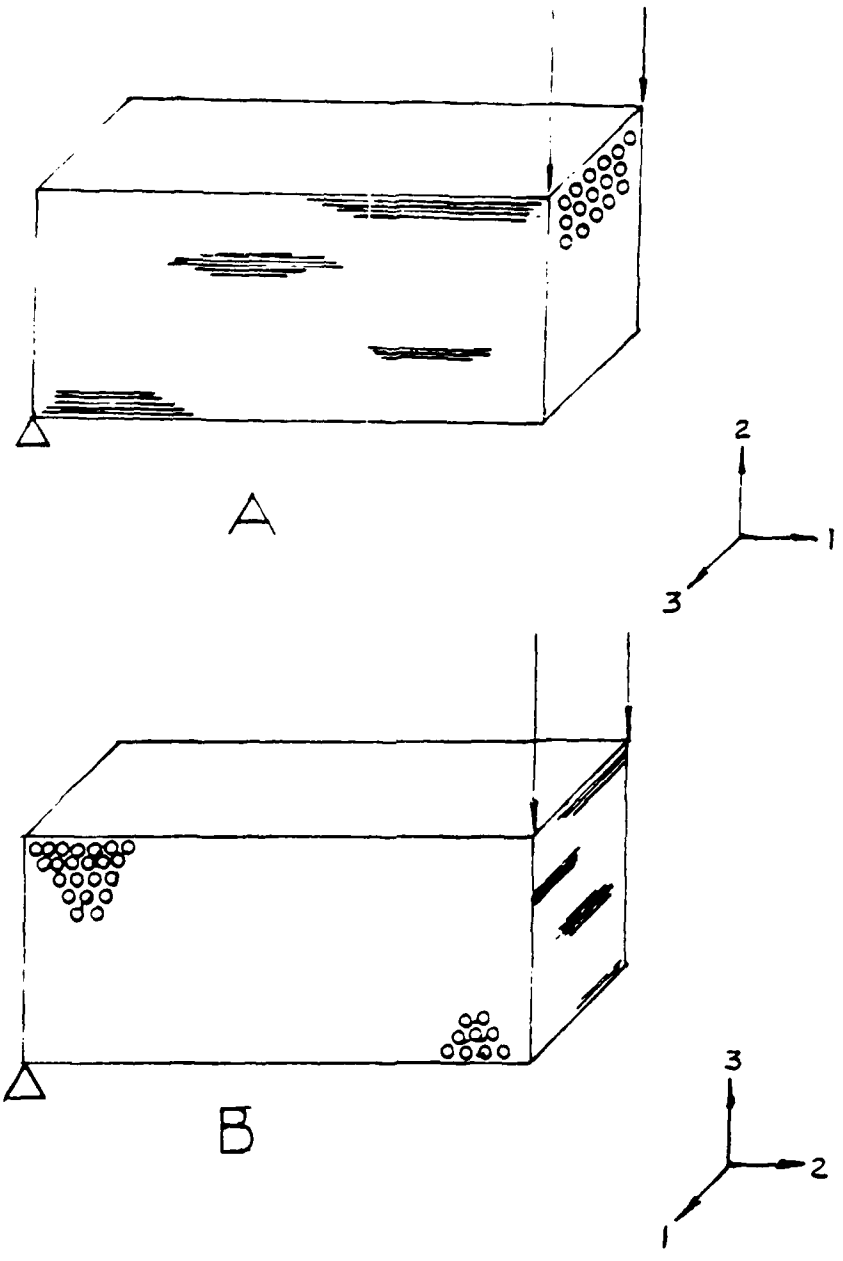

Fiber Orientation Directions

(a) Zero Degrees, (b) Ninety Degrees

Fig. 2

expect that the ninety (90) degree orientation would act most like isotropic materials because of the in-plane symmetry.

Finite Element Model

The essential parts of a finite element analysis include the code and the modeling. This research employed the NOSAPM code, a modified version of NONSAP. The Aeropropulsion Laboratory of the Air Force Wright Aeronautical Laboratories (AFWAL) developed NOSAPM to model bird strikes on turbine engine blades.(15) NOSAPM is a multipurpose finite element code capable of nonlinear and linear static and dynamic analysis. NOSAPM uses a displacemental formulation

$$[K]\{U\} = \{R\} \tag{5}$$

where the stiffness matrix K is

$$[K] = \sum_{m} \int_{V^{(m)}} B^{(m)T} E^{(m)} B^{(m)} dV^{(m)} \tag{6}$$

with B dependent on the shape function and E the material properties of the element. The vectors U and R are the

displacements and loads, respectively. A one dimensional truss and a three dimensional quadrilateral element are available in NOSAPM. The element properties range from linear elastic to elastic-plastic. A linear orthotropic model exists which is appropriate for representing composite materials. The stress-strain relationship for this orthotropic model is

$$\begin{pmatrix} \epsilon_1 \\ \epsilon_2 \\ \epsilon_3 \\ 2\epsilon_{12} \\ 2\epsilon_{23} \\ 2\epsilon_{13} \end{pmatrix} = [C] \begin{pmatrix} \sigma_1 \\ \sigma_2 \\ \sigma_3 \\ \sigma_{12} \\ \sigma_{23} \\ \sigma_{13} \end{pmatrix} \tag{7}$$

where C, the compliance or inverse stiffness matrix is

$$\begin{pmatrix} 1/E_a & -\nu_{ab}/E_b & -\nu_{ac}/E_c & & & \\ -\nu_{ba}/E_a & 1/E_b & -\nu_{bc}/E_c & & & \\ -\nu_{ca}/E_a & -\nu_{cb}/E_b & 1/E_c & & & \\ 0 & 0 & 0 & 1/G_{ab} & & \\ 0 & 0 & 0 & 0 & 1/G_{ac} & \\ 0 & 0 & 0 & 0 & 0 & 1/G_{bc} \end{pmatrix} \tag{8}$$

Note, the Young's moduli, shear moduli, and Poisson's ratios are with respect to the material axes. Thus, based on the

material model chosen, NOSAPM will determine the displacements first and then calculate the stresses based on these displacements. In addition to its material and elemental capabilities, NOSAPM reformulates the stiffness equations at the user's request during a nonlinear analysis and performs the necessary equilibrium calculations to account for large displacements.

As mentioned earlier, the short beam shear test was the configuration used in this study of damage initiation. In modeling the beam for the short beam shear test, the three dimensional quadrilateral element was used. Each of these "brick" elements contained eight nodes, one for each corner of the element. The coordinate system chosen uses "x" for the thickness, "y" for the length, and "z" for the depth of the beam, as well as for the direction of the load (Fig. 1). With this study only two dimensions, y and z, were left unconstrained thus creating a plane strain case. With a displacemental solution, this restriction allows movement in only two directions reducing the three dimensional element to two dimensions. Note that this plane strain configuration will result in higher stresses than the plane stress cases of Copp and Keer (5) used for validation. The basic shapes of the stress contours should be sufficiently close enough for the comparisons.

The final mesh geometry representing the beam is shown in Figure 3. As shown, the model consists of fourteen (14) elements through the thickness with eleven (11) elements along the beam axis for a total of fifty-four (54) elements. The model is only one element thick. Since eight noded brick elements are employed, the total number of nodes is 360. A convergence study determined that the element mesh should be refined directly under the load in order to accurately model the strong stress gradients in this area. The model takes advantage of symmetry along the centerline of the beam, under the load. Symmetry is required because of model size limitations of the code and a desire to conserve computer resources. The support is modeled as a constraint in the "z" direction, while the symmetry nodes along the edge are constrained from moving in the "y" direction. All nodes are constrained in the "x" direction.

Damage Criteria

With the model established, the next step is to incorporate the damage criteria into the computer code. Several different criteria were considered that have been demonstrated to model failure or damage in a composite material under simple loads. These included maximum stress,

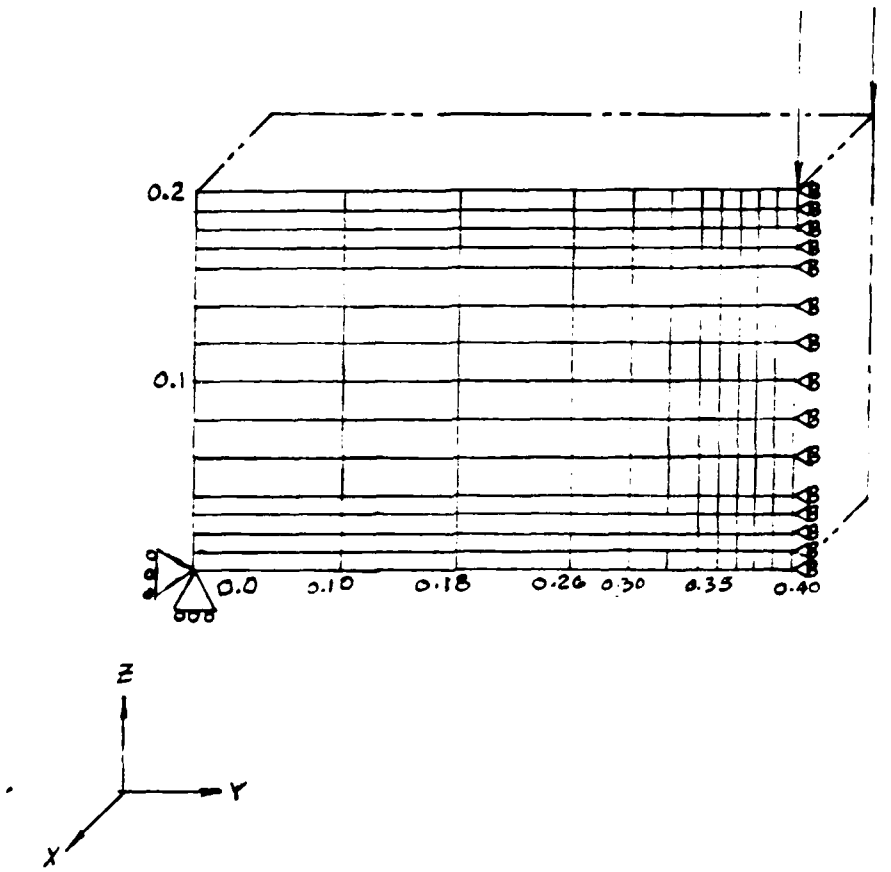

Finite Element Model Mesh Geometry

Fig. 3

Tsai-Hill, and Tsai-Wu. With the beam test configuration, the state of stress will be three dimensional and interdependent. The failure criteria must consider the influences of all the stress components. Thus, either the Tsai-Hill or the Tsai-Wu appear to be the most attractive candidates. The Tsai-Hill theory was chosen for its simplicity and ease of adaptation to the beam test problem. Also, with the lamina orientation in only two directions of zero (0) and ninety (90) degrees, the Tsai-Wu theory would reduce to Tsai-Hill theory for this orientation and geometry. The Tsai-Hill equations are found in Jones (8:76-79) as follows:

$$(G+H)\sigma_1^2+(F+H)\sigma_2^2+(F+G)\sigma_3^2-2H\sigma_1\sigma_2-2G\sigma_1\sigma_3-2F\sigma_2\sigma_3 + 2L\tau_{23}^2+2M\tau_{13}^2+2N\tau_{12}^2=1 \qquad (9)$$

The strength parameters are F, G, H, L, M, and N which relate to material strength properties X, Y, Z, and S. These relationships are:

$$2N=\frac{1}{S_{12}^2}$$

$$2M=\frac{1}{S_{13}^2}$$

$$2L=\frac{1}{S_{23}^2} \qquad (10)$$

with S being the shear strength in the respective directions,

$$G + H = \frac{1}{X^2}$$

$$F + H = \frac{1}{Y^2}$$

$$F + G = \frac{1}{Z^2} \qquad (11)$$

Note, X, Y, and Z are the tensile or compressive strengths along the respective material axes. The remaining three terms for the cross product relationships are:

$$2H = \frac{1}{X^2} + \frac{1}{Y^2} - \frac{1}{Z^2}$$

$$2G = \frac{1}{X^2} + \frac{1}{Z^2} - \frac{1}{Y^2}$$

$$2F = \frac{1}{Y^2} + \frac{1}{Z^2} - \frac{1}{X^2} \qquad (12)$$

For the purpose of this analysis the tensile and compressive strengths of each axis are assumed equal.

Along with a correct determination of the stress fields the damage criteria is critical in the study of damage ini-

tiation. Damage initiation begins at the point when the damage criteria is exceeded. Subsequent work is not intended to analyze the stress and displacement fields in the immediate vicinity of the damage. Instead, the analyses reflect the containment of the damaged zone by the surrounding elastic structure. The progression of the damage zone into this elastic field is one of the principle interests of this research.

The Tsai-Hill failure criteria is incorporated into NOSAPM through the subroutine DAMAGE. A discussion and documentation of this subroutine is given in Appendix 2. Briefly, the material strength properties are input along with the other material characteristics. A control card parameter determines which criteria will be used. Currently, DAMAGE includes only the Tsai-Hill criteria. It should be noted that any desired criteria could be easily added. As NOSAPM calculates the stresses for an element with each step, DAMAGE checks the element's stress field against the criteria. If the stress field exceeds the criteria, the element is considered damaged and is so noted with another control parameter in NOSAPM. Elements are checked against the criteria individually and designated as damaged accordingly. A damaged element can then be modified as appropriate using reduced stiffnesses or some other mechanism.

Stiffness Reduction

As a material fails, its resistance to deformation and its ability to carry loads decreases. One way this can be characterized is by a reduction in the material's elastic properties. This reduction is intended to model the material cracking and crushing that occurs locally but precedes the catastrophic failure of delamination. With the finite element approach taken, an element was considered failed when the stresses within the element combined to exceed the Tsai-Hill criteria described earlier. While this thesis concentrated on the initiation of damage, an insight into the progression of such damage is possible. By tracking element failures and making the appropriate stiffness modifications one can discern a damage growth pattern. This pattern qualitatively describes the damage and can be explained by examining the surrounding stress fields. Although the damaged elements do not accurately reflect the singular stresses present due to cracks or plastic deformation, the results do coincide with experimentally observed damage.

Stiffness reduction is accomplished by changing the material properties of the element. With the input file several sets of material properties can be specified to describe the successive decreases in stiffness. The first set

defines the material properties in the undamaged state The next set of properties is a reduction of the first set by some predetermined percentage. The following sets can be further reduced as desired. Since the stiffness is directly determined from the material properties, it decreases as the properties decrease. A control variable within NOSAPM calls a new set of properties after damage occurs and with each subsequent stiffness reformation. The result is an element triggered by exceeding some failure criteria reducing in stiffness. As the loading continues, the element stiffness can continue to be reduced through the use of additional sets of material properties.

Stiffness reduction was implemented two different ways. The first was a reduction which occurred with each step in the program. The stiffness was gradually reduced to model an increase in damage to elements previously failed. Thus, at any step the element(s) which failed first would be softer than elements just failing. The second method of stiffness reduction employed was to impose the entire reduction at once. Any increase in program steps would have no additional effect on failed elements. This method was employed to model complete crushing and cracking of an element constrained only by the surrounding elastic field.

Stress Field

The beam bending problem analyzed represents a stress field with a combination of local and global stresses. The local stresses are a result of the point load and the supports. The global stresses are the beam bending stresses contained in any beam problem. The combinations of these stresses determine the failures. Three stresses, normal, bending, and shear, are important in this two dimensional representation of the short beam shear test. These stresses, shown in Figure 4, will then be combined through the Tsai-Hill relationships to determine damage/failure.

NOSAPM, like most finite element programs, calculates the stresses in each element by first determining displacements. The displacements then become strains and Eq (7) calculates the stresses using these strains. The stresses as well as displacements are then tabulated by the program with the output. A large mesh with many elements produces a large table of stresses for each step in the analysis. These tables are useful, but cumbersome.

Post-processing is usually required to transform the raw data into a more usable form. For this analysis stress contours of the stresses calculated at Gauss points in each element were plotted by a program called SURFER, a graphics program designed to produce contours and surface plots.

NOSAPM required some modifications to produce files compatible with SURFER so that it could be utilized as a post-processor. Appendix 1 describes these NOSAPM modifications and the resulting output files. With the contour plots, the pages of stresses are reduced to single pictures for rapid data reduction.

Each stress contour is important in the determination of damage progression through the short beam shear model. Failure mode determinations from testing usually assume the absence of some stresses or the dominance of other stresses. For example, a typical tensile strength test eliminates all stresses but tension. The short beam shear test assumes that the transverse shear stress dominates and results in a delamination failure defining interlamina shear strength properties. Finite elements will allow for calculation of each stress component. Modifications to NOSAPM, mentioned earlier, permit these stresses to be combined by the Tsai-Hill criteria to define failure. Failure can then be characterized, and the dominant stresses identified. Only then can a failure mode be deduced and the damage progression displayed. Normal, bending, and shear stress contours are shown, as well as the Tsai-Hill stress field.

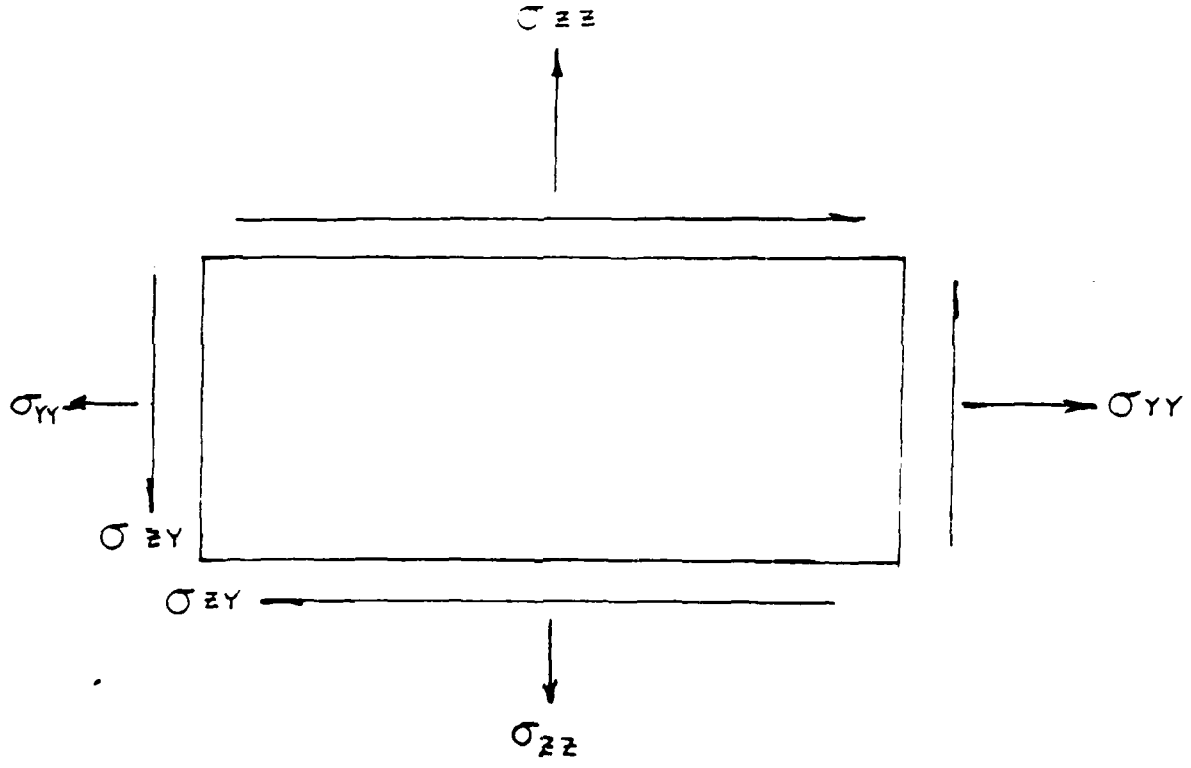

Stresses Analyzed for Damage Criteria

Fig. 4

IV. Results and Discussion

The finite element program, NOSAPM, combined with the graphics program, SURFER, produced contour plots to evaluate the short beam shear test. Stress fields were developed to compare with other more exact solutions. Damage zones plotted were based on the Tsai-Hill failure criteria. The contours also helped to evaluate the stiffness reduction techniques as a method of determining damage initiation. The results below attempt to satisfy the objectives of obtaining the complex stress fields of this mixed boundary value problem, applying a failure criteria to the problem, and using stiffness reduction to model damage initiation. It should be noted that with each contour plot only a small portion of the beam is presented as shown in Figure 5. This section is under the load and along the line of symmetry in the computer model. In this region, the local stresses are most significant. Also, this region contains occurrences of observed local failures. The finite element mesh has been optimized to model the stress gradients in this region and to conserve computer resources.

Shear Test Stress Fields

The first objective of this study was to determine

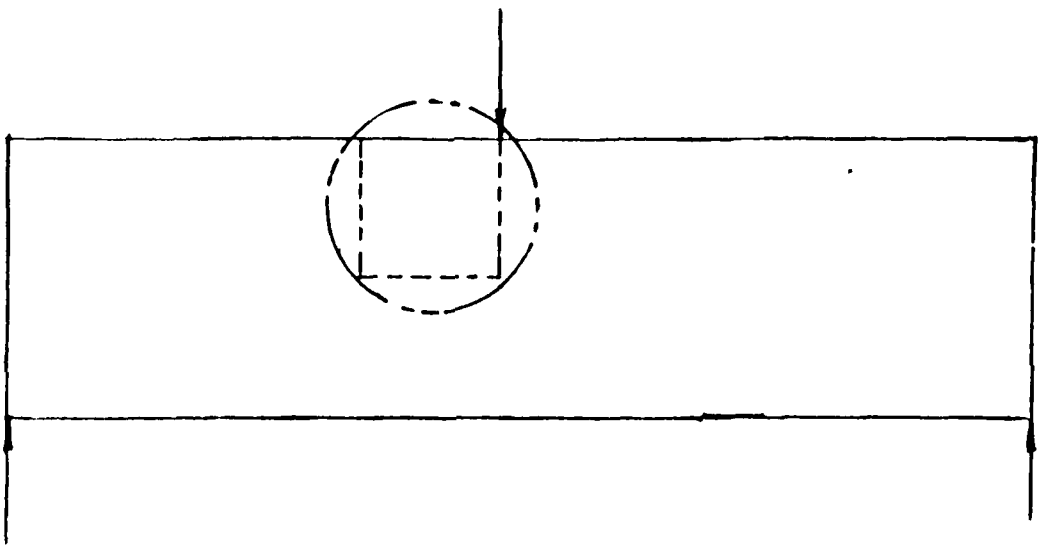

Section of Beam Stress Field Plotted

Fig. 5

the stress fields of the short beam shear test. High stress gradients were expected around the area of load application. Thus, the greatest refinement of the element mesh should be in this area. A convergence study demonstrated this need for refinement and resulted in the mesh shown in Figure 3. The mesh emphasizes the outer fibers of the beam as well as the area directly below the applied point load. Both the ninety degree and the zero degree fiber orientations were used. The resulting stress contours show patterns similar to those obtained by Copp and Keer (5) using a more exact numerical technique.

The normal stresses for both the ninety and zero degree cases are shown in Figures 6 and 7. As indicated by Copp and Keer (5:123,124), these stresses are dominated by the point load and the support reaction. Although not seen with the beam section shown, these normal stresses for both ninety and zero degree cases disappeared in the center region of the beam away from the load and reaction. Note that the normal stress contours for the zero degree case do appear to be tighter in the vicinity of the load point than the ninety degree case. However, the deviation is small.

Shear values for the same cases are shown by Figures 8 and 9. The zone of highest shear is seen to

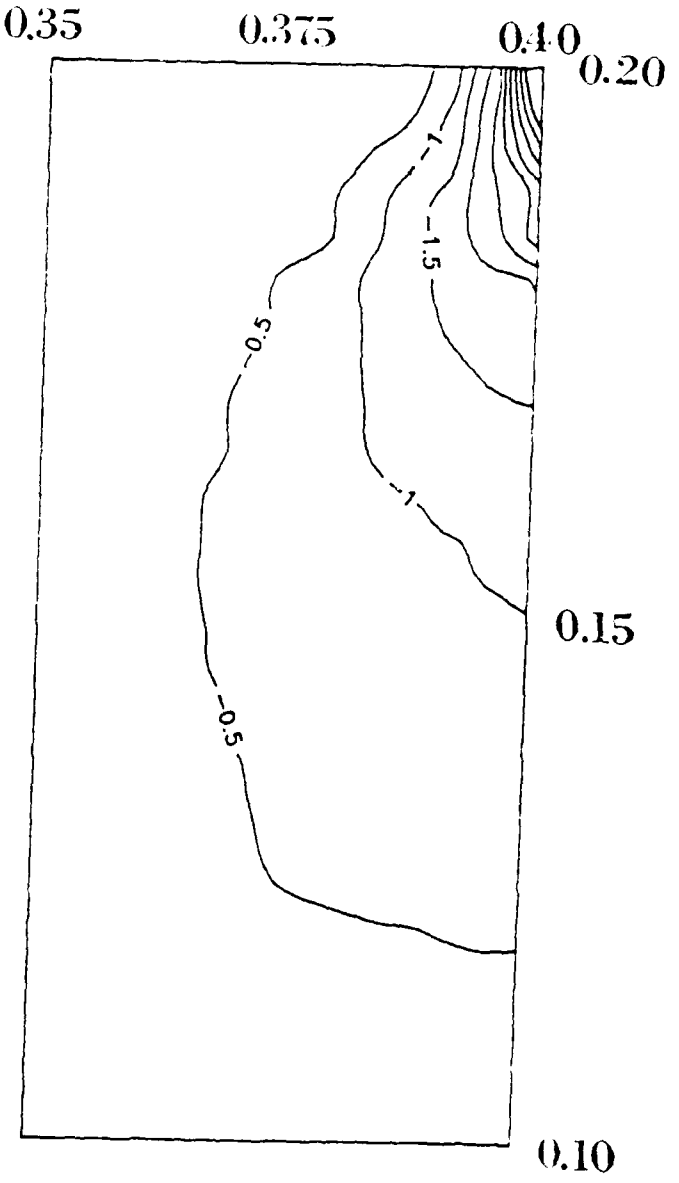

P = 20 lb, Normal Stress

Ninety Degree Fiber Orientation

Fig. 6

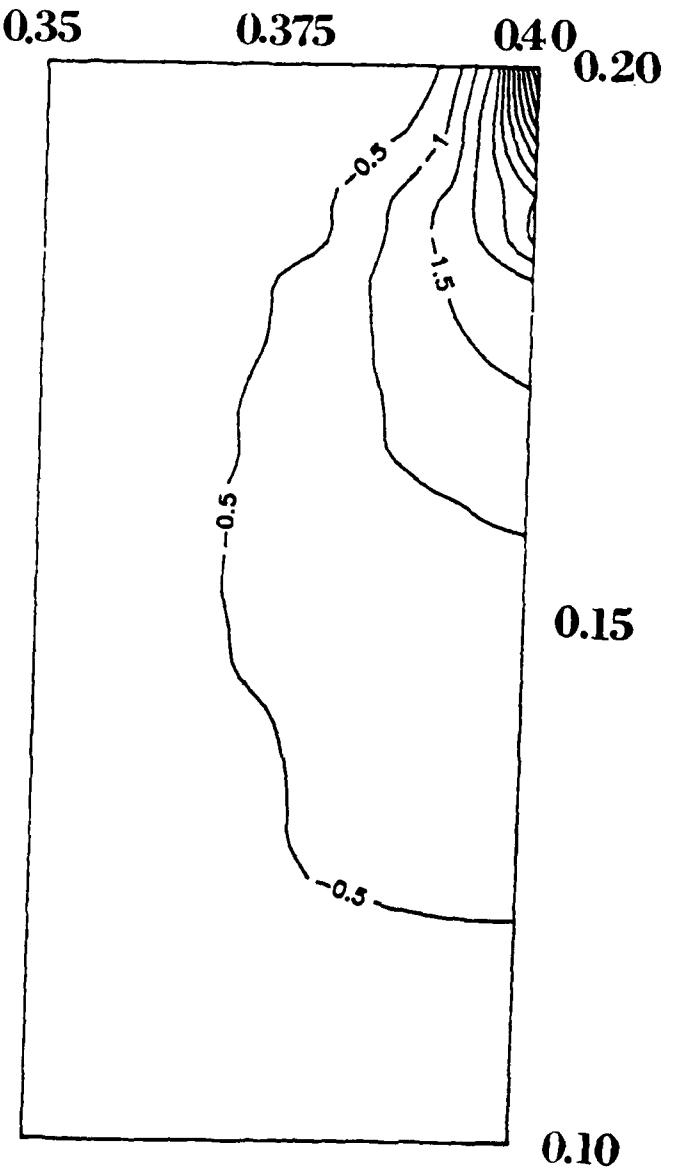

P = 20 lb, Normal Stress

Zero Degree Fiber Orientation

Fig. 7

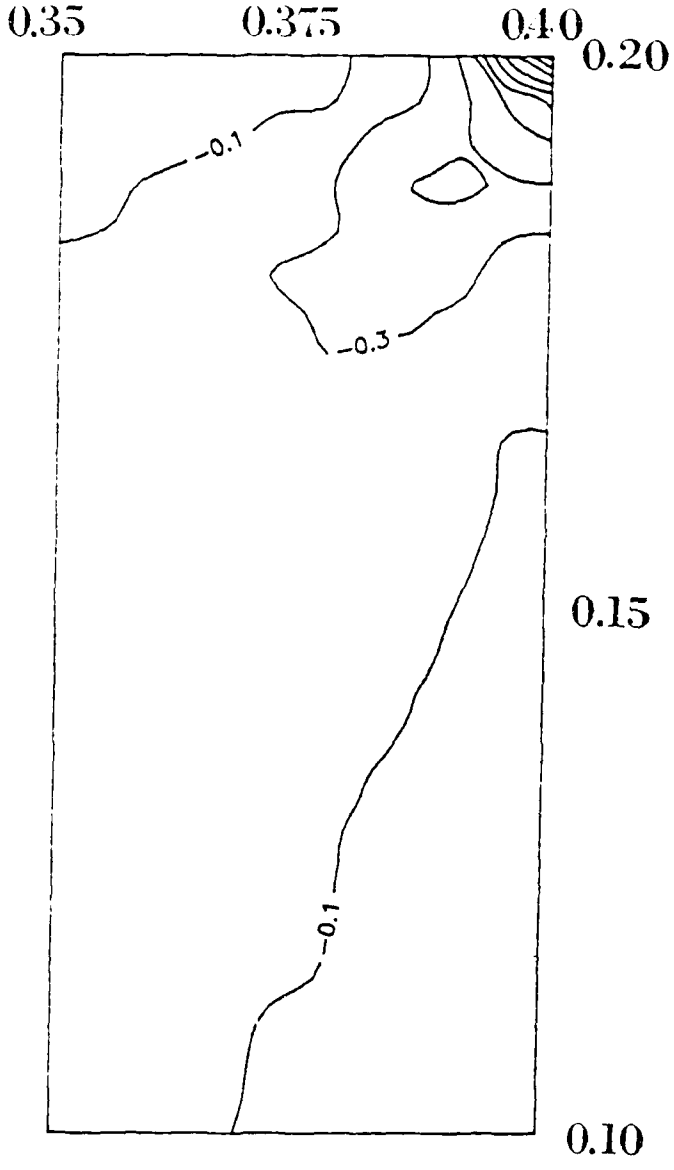

P = 20 lb, Shear Stress

Ninety Degree Fiber Orientation

Fig. 8

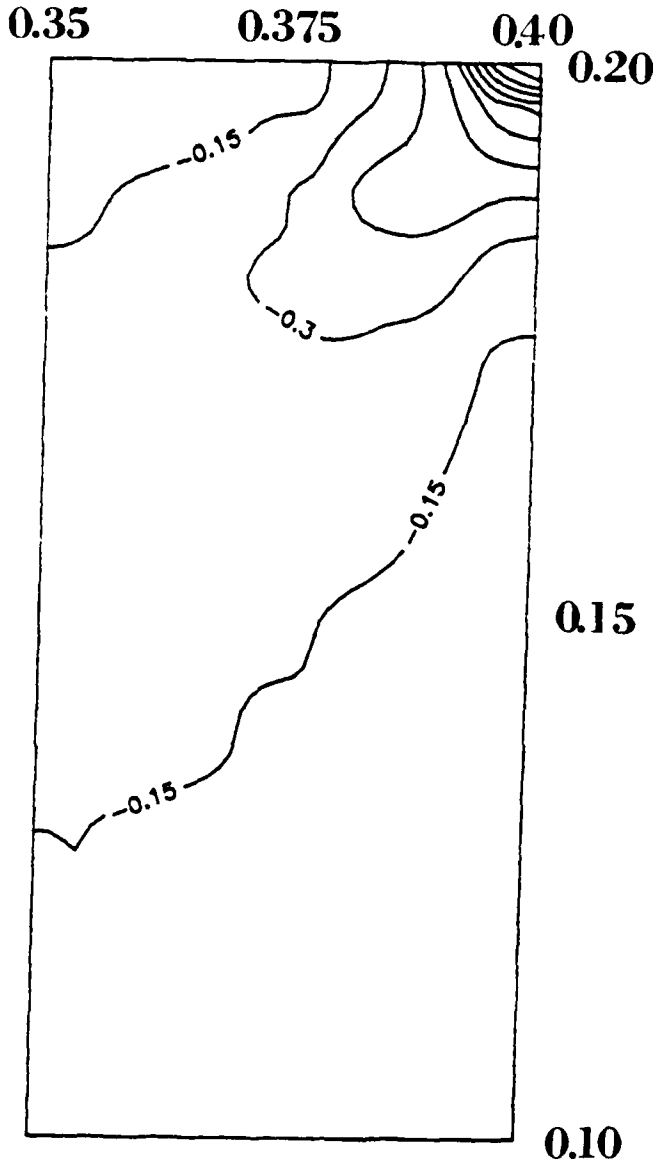

P = 20 lb, Shear Stress

Zero Degree Fiber Orientation

Fig. 9

vary from the load point to the center line as expected from beam theory and observed by Copp and Keer (5:126,127). Unlike the normal stresses, the shear stresses closely agree for the two cases. These shear contours were the most difficult to obtain. Away from the refined mesh area these contours wavered and became ill-defined. While the displacements were compatible across element borders, the shear stresses across these boundaries were not. The high shear gradients around the load required a very fine mesh to obtain stress contours as detailed as Copp and Keer.

Bending stress contours, on the other hand, were relatively easy to generate. The ninety and zero degree bending cases are seen in Figures 10 and 11. The neutral axis appears along the centerline of the beam as expected. Although not shown with these sections, the stresses appear symmetric about a neutral axis with a little distortion around the point load, also matching the patterns found by Copp and Keer (5:129,130). Beam theory clearly predicts the symmetry about a neutral axis. The distortion around the point load area is easy to understand since the local displacements caused by the loading are not linear with respect to the rest of the beam's displacement.

So, with the exception of the area away from the refined

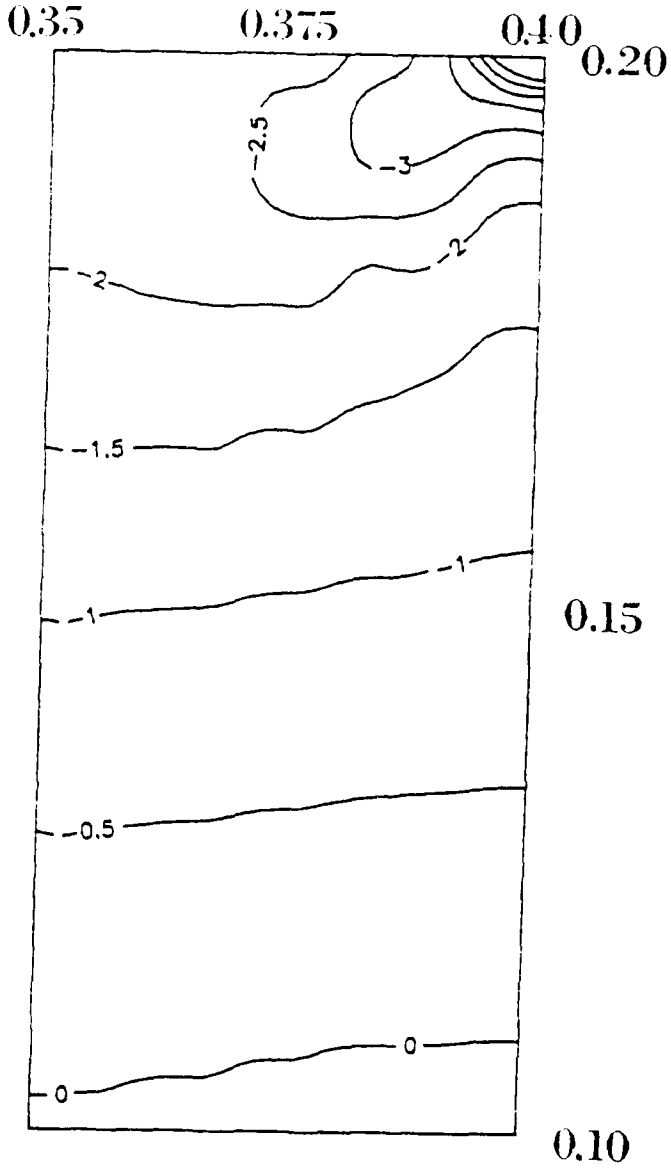

P = 20 lb, Bending Stress

Ninety Degree Fiber Orientation

Fig. 10

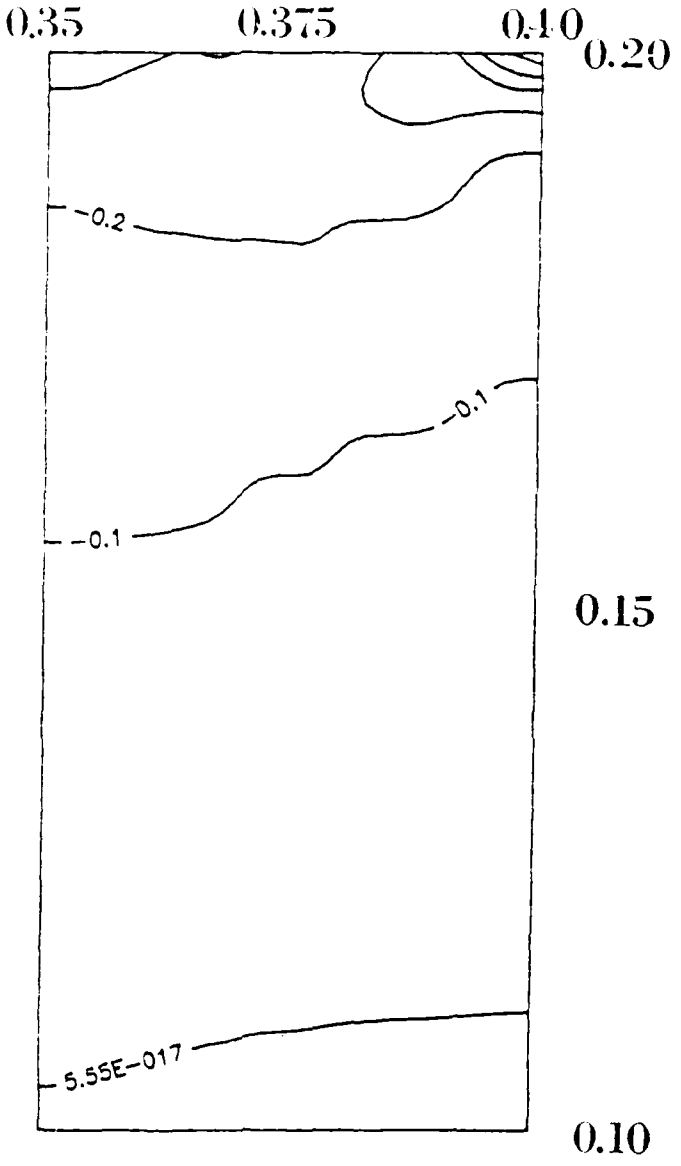

P = 20 lb, Bending Stress

Zero Degree Fiber Orientation

Fig. 11

mesh, the stress contour patterns seem to be in agreement with the work of Copp and Keer (5). A similar but dynamic load case was studied by Murthy and Chamis (9) resulting in contour patterns close to those shown here. It now seems reasonable that NOSAPM along with the mesh used can determine the complex stress fields associated with the short beam shear test around the area of loading.

Damage Criteria in NOSAPM

The Tsai-Hill criteria was used as the means of determining elemental failure. The subroutine DAMAGE (see Appendix 2) compared the current stress fields in each element with the material's strengths. Damage occurs when the combinations of stresses and strength ratios are greater than one (1). The resulting plots for both the ninety and zero degree cases show a state of stress past initial failure. Figures 12 and 13 show stress combinations exceeding the Tsai-Hill criteria with values greater than one. The overload case may be somewhat artificial in the sense that material degradation would already have occurred and the failure pattern would probably experience some change. However, the overload cases are a good comparison to the works of Copp and Keer (5:140,141).

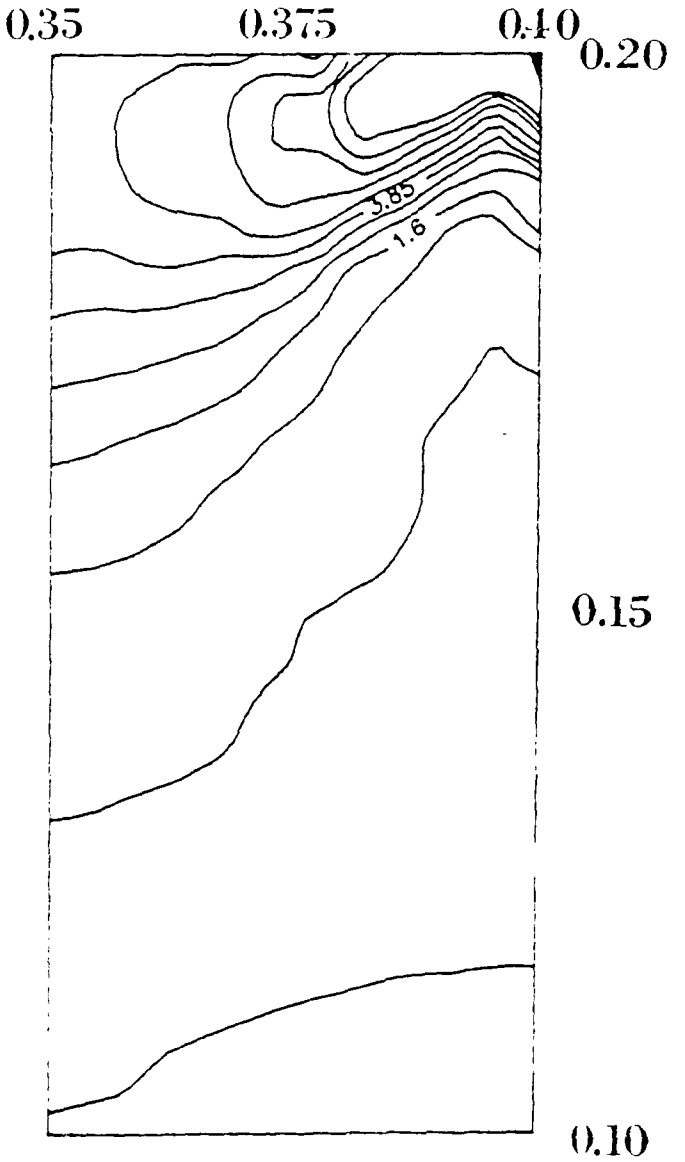

P = 20 lb, Ninety Degree Fiber Orientation

Eq (9), Tsai-Hill

Fig. 12

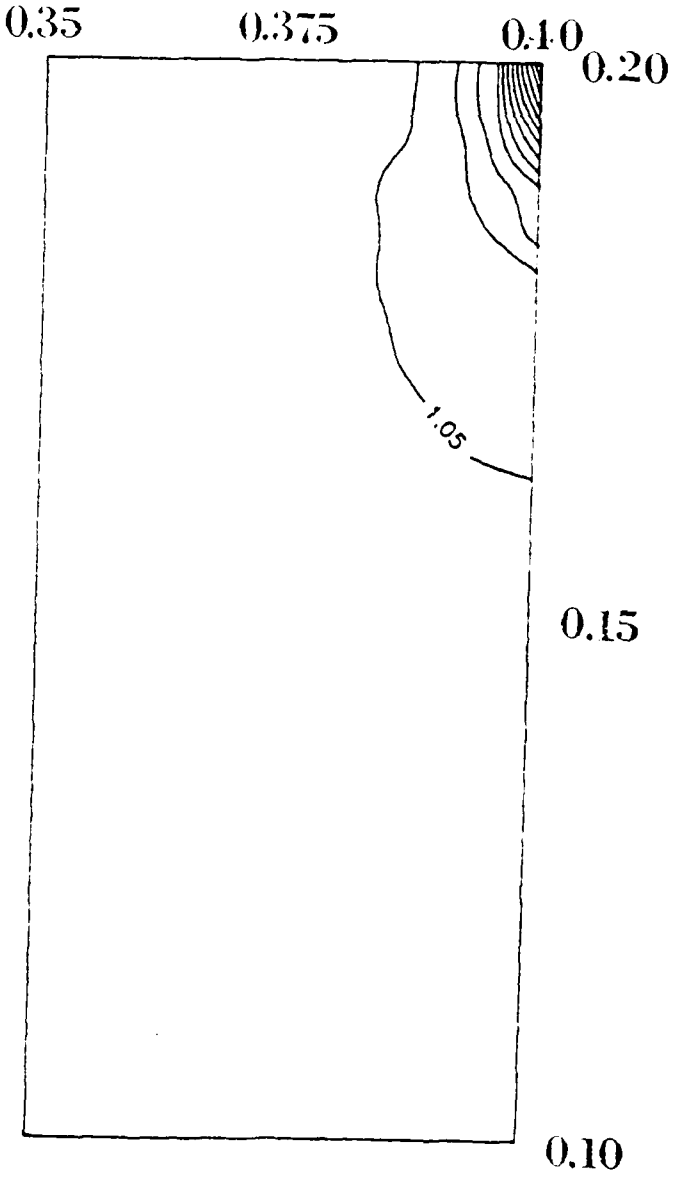

P = 20 lb, Zero Degree Fiber Orientation

Eq (9), Isai-Hill

Fig. 13

The ninety degree case represents material that is isotropic, especially in the plain strain configuration studied. The failure pattern shown (Figure 12) closely resembles the bending stress contours (Figure 8). This pattern shows some localized effects from the load, but primarily the failure exhibited is beam bending. The zero degree case is representative of anisotropic or composite materials. Its failure pattern (Figure 13) most closely matches the normal and shear stress cases (Figures 9 and 10). This indicates that the predominant failure modes are normal and shear with the load application point the major contributor. The absence of the beam bending patterns in this case suggests that normal beam theory is not applicable. The extremely high failure values near the load point seem to reinforce the theory by Whitney and Browning (19) that the short beam shear test possesses a more complex stress field than beam theory predicts. The next step in this damage initiation study was to model damage by reducing the stiffness in the failed element(s).

Stiffness Reduction in NOSAPM

Stiffness reduction was incorporated into NOSAPM using

the subroutine DAMAGE and the code's ability to handle a number of different sets of material constants. Property sets were read into NOSAPM with the moduli reductions corresponding to desired stiffness reductions. For example, if a twenty percent reduction was needed, the first set of material properties would be the originals and the second set would be values reduced by twenty percent. The Poisson's ratio would remain the same, while the Young's modulus and shear modulus would be reduced by twenty percent. When DAMAGE determined a "failed" element, NOSAPM would then assign the second set of properties to that element while the other elements retained their original values.

This stiffness reduction technique affects the entire element once failure occurs. First, the technique was checked with a simple single element compression case. Then, the technique was used with the short beam shear test model with fibers oriented in both the zero and ninety degree configurations. Two questions are addressed with this study. The first is whether the technique works with the finite element code NOSAPM. The second question deals with the applicability of modeling damage initiation by reducing the stiffness of the entire element.

Single Element Compression. As a test of the stiffness reduction modifications to NOSAPM a single element under

simple compression was investigated. The element was constrained on three sides with a compressive load in the "z" direction (Figure 14). The load was held constant while the stiffness was reduced five percent (5 %) with each solution step. Simple mechanics theory provided the predictions for displacements and stresses.

To begin with, the displacements for the single element can be found using the axial deformation equation:

$$\delta = \frac{PL}{AE} \tag{13}$$

where **P** is the load, **L** is the original length, **A** is the original area, and **E** is the Modulus of Elasticity. The load remained constant during the entire run. The length and area can be considered constant since the changes caused by the load considered are small with respect to the original dimensions. With the above assumptions, one would then expect the deflection to be inversely proportional to the modulus.

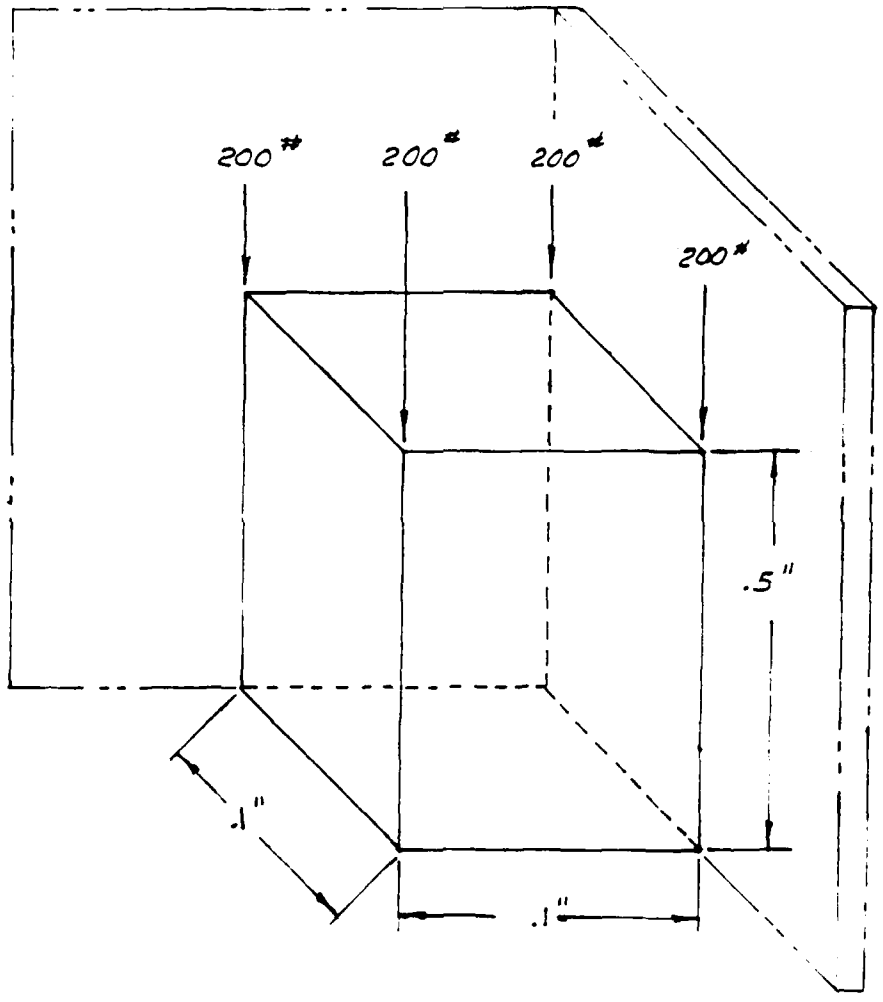

Single Element Compression Check Configuration

Fig. 14

Another parameter to check with the program is the stress. In this simple configuration, the stress can be approximated by the axial stress equation:

$$\sigma = \frac{P}{A} \tag{14}$$

As mentioned earlier, the load is constant and the area is assumed unchanged. The stress within the single element can then be expected to remain constant as it is independent of any modulus change.

The results of this check case on the behavior of the stiffness reduction scheme are shown in Table 2. The calculated displacements do not vary from theory except for slight round-off and truncation differences. The only stress possible, that in the "z" direction, remained constant as predicted. These results give confidence that the stiffness reduction scheme does not interfere with the displacemental solutions of NOSAPM and correctly computes stresses based on the most current stiffness moduli values.

Zero Degree Fiber Orientation. The effects of stiffness reduction as a possible model of damage initiation in composites was studied using a short beam shear test configura-

tion developed earlier with fibers in the zero degree orientation. This parametric study included two extremes. The first was a constant load with a varying reduction. The second increased the load while keeping the reduction fixed. These two cases provided bounds for this reduction technique.

Single Element Check
for
Stiffness Reduction
Table 2

Young's Modulus (psi)	Calculated Displacement (in)	NOSAPM Displacement (in)	Calculated Stress (psi)	NOSAPM Stress (psi)
30.0×10^6	0.001333	0.0013333	80,000	80,000
28.5×10^6	0.001404	0.0014035	80,000	80,000
27.0×10^6	0.001481	0.0014814	80,000	80,000
25.5×10^6	0.001569	0.0015686	80,000	80,000
24.0×10^6	0.001667	0.0016667	80,000	80,000

As stated earlier, the first case kept a constant load with a varying stiffness reduction. This constant load of three (3) pounds was chosen as it represented the first indication of damage occurrence. NOSAPM showed the element directly under the load failing at the integration point nearest to the load. The output file, TAPE30, was then used to track any changes to element failure with stiffness reductions. TAPE30 and other input/output files are explained further in Appendix A. Stiffness reductions produced the threshold of damage initiation in the element. The progression of damage into the body can only be observed by noting the increase in the stress fields of the adjacent elements as shown in Figures 15, 16, and 17. From 100% (Figure 15) to about 50% of the original stiffness, the failed element does not change as stresses at only one integration point exceeded the Tsai-Hill criteria. The damage contour shows the dominance of the normal stress. Between 50% (Figure 16) and about 5% of the original stiffness, stresses at two integration points within the element exceed the Tsai-Hill criteria. Contour lines tighten up around the load but seem to spread out more through the beam. A stiffness reduction smaller than 5% (Figure 17) of the original stiffness transfers the load through the element in such a way that

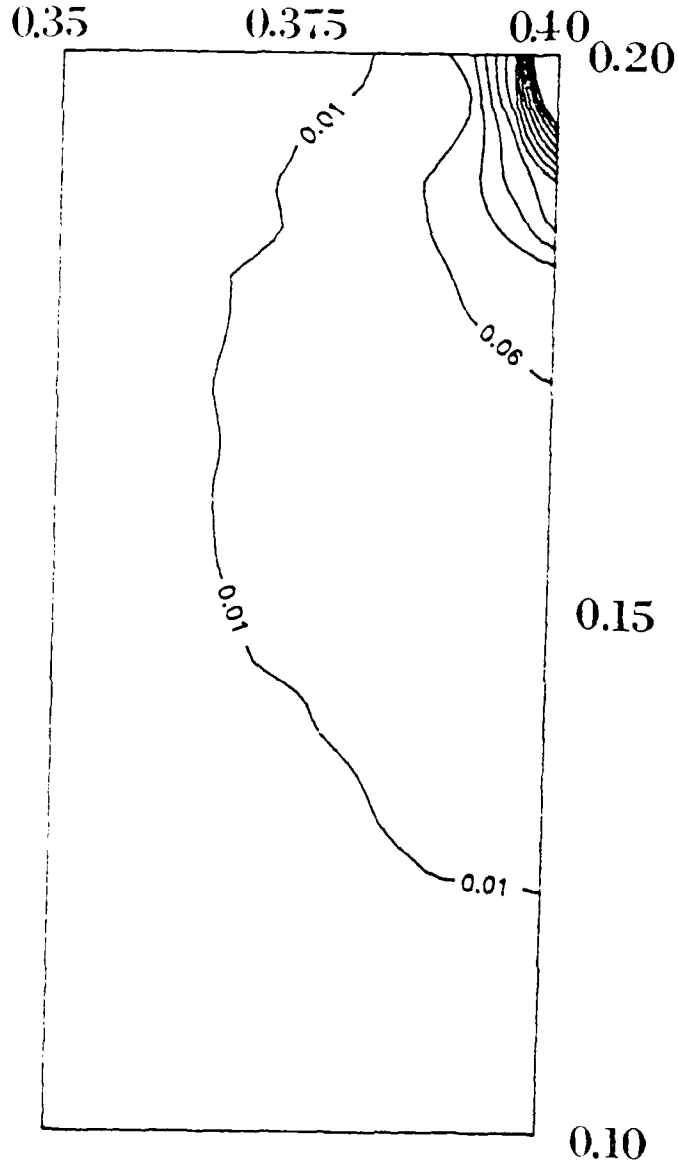

Eq (9), Tsai-Hill, 0% Stiffness Reduction

Constant Load, P = 3 lb

Fig. 15

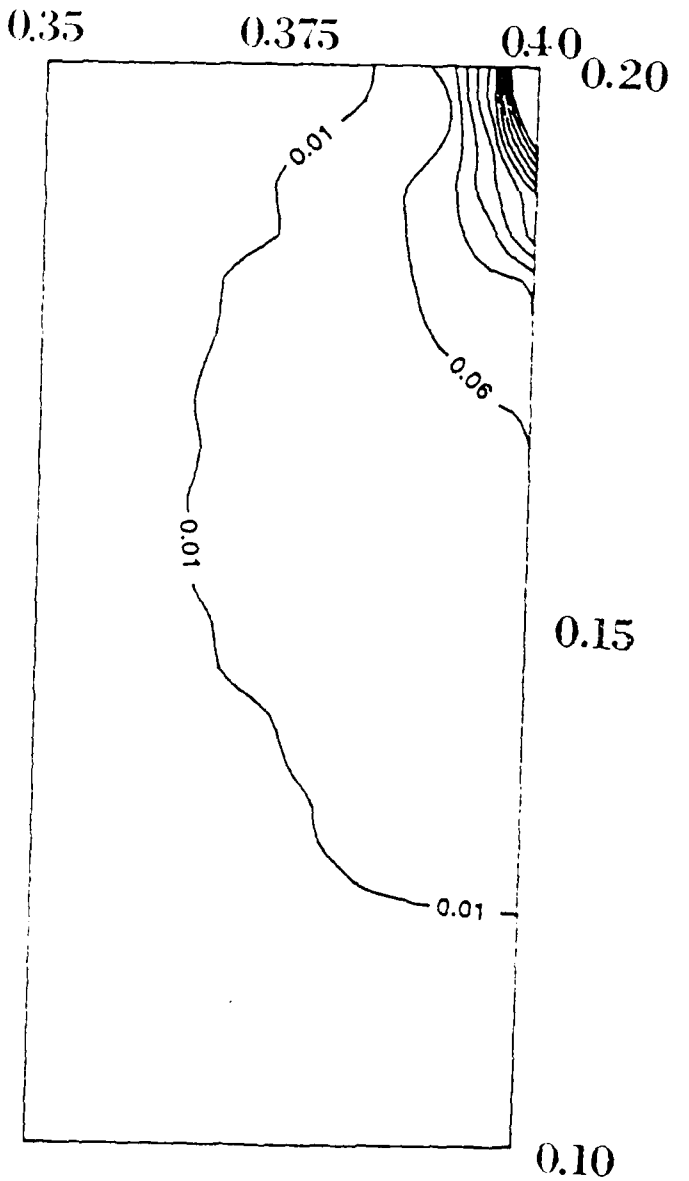

Eq (9), Tsai-Hill, 50% Stiffness Reduction

Constant Load, P = 3 lb

Fig. 16

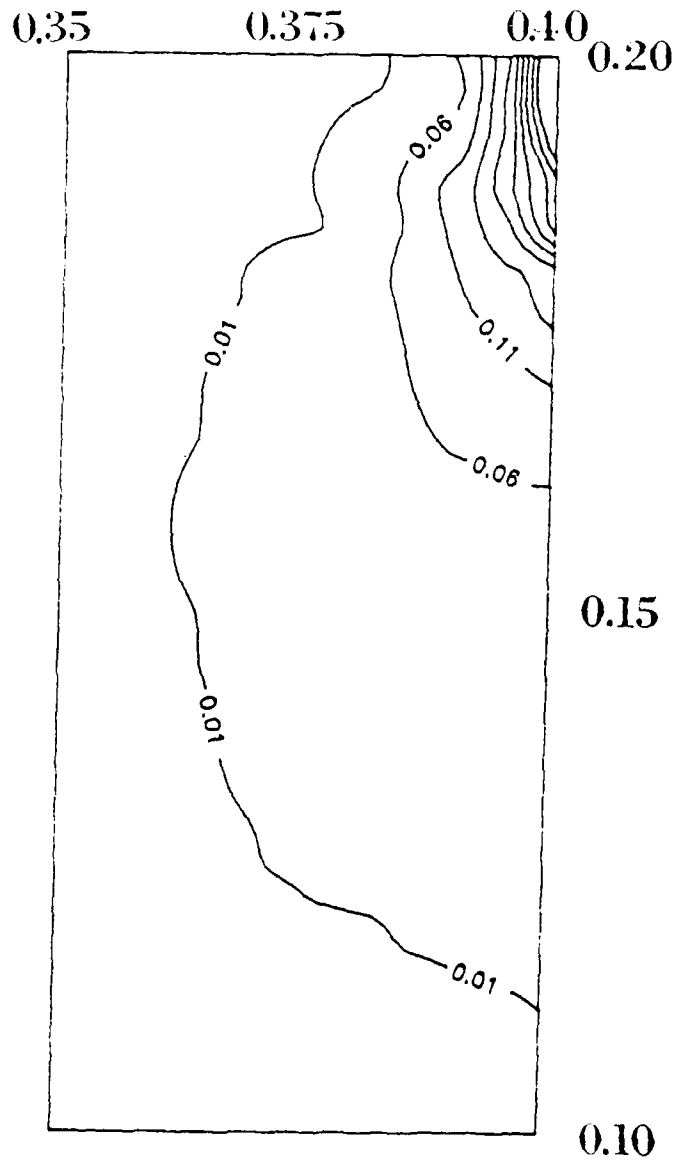

Eq (9), Tsai-Hill, 95% Stiffness Reduction

Constant Load, P = 3 lb

Fig. 17

no failure occurs within the element. In other words, stresses within the reduced stiffness element at all integration points fall below the failure criteria of Tsai-Hill. The intensity of the applied load as shown in the Tsai-Hill plots appears to be spread into the beam, reducing the stresses in the originally failed element.

The normal and shear stress contours remain the same shape regardless of stiffness reduction. Some differences can be seen from the full stiffness case (Figures 18 and 19). Stiffness reduction appears to affect the normal stresses by shifting them away from the load point as shown in Figures 20 and 21. The maximum normal stress is lower with the larger reduction, but higher stresses are spread further in the beam (Figure 21). The same is true for the shear stress. With the fifty percent reduction case (Figure 22), the shear increases around the load. As the stiffness is reduced further to five percent of its original stiffness (Figure 23), the shear decreases around the load while increasing in the surrounding elements. The increasing shear seems to be moving towards the centerline of the beam. This behavior does correlate with observed patterns of failure in short beam shear tests (20). Maximum shear is expected

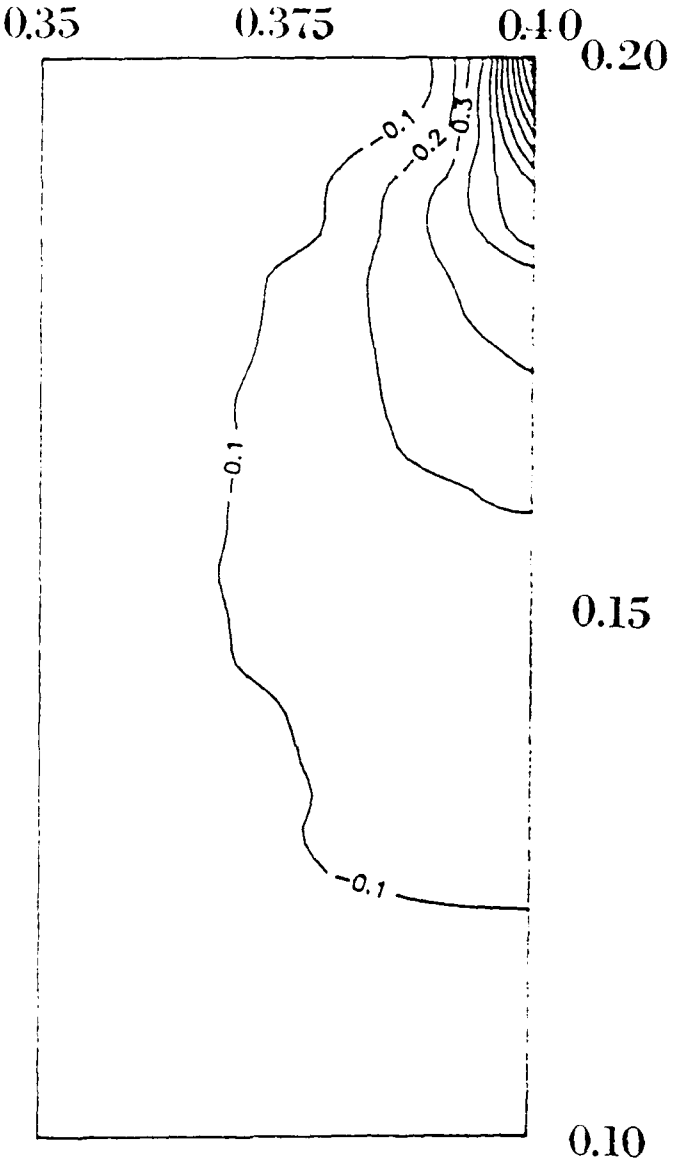

Normal Stress, 0% Stiffness Reduction

Constant Load, P = 3 lb

Fig. 18

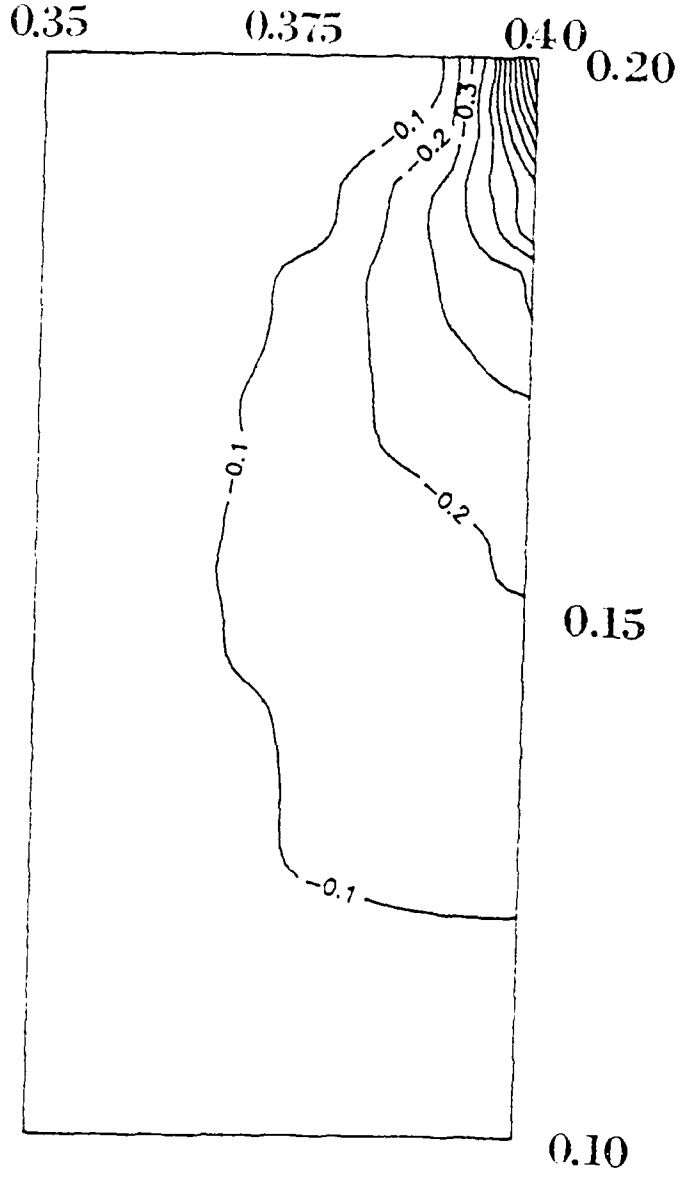

Normal Stress, 50% Stiffness Reduction

Constant Load, P = 3 lb

Fig. 19

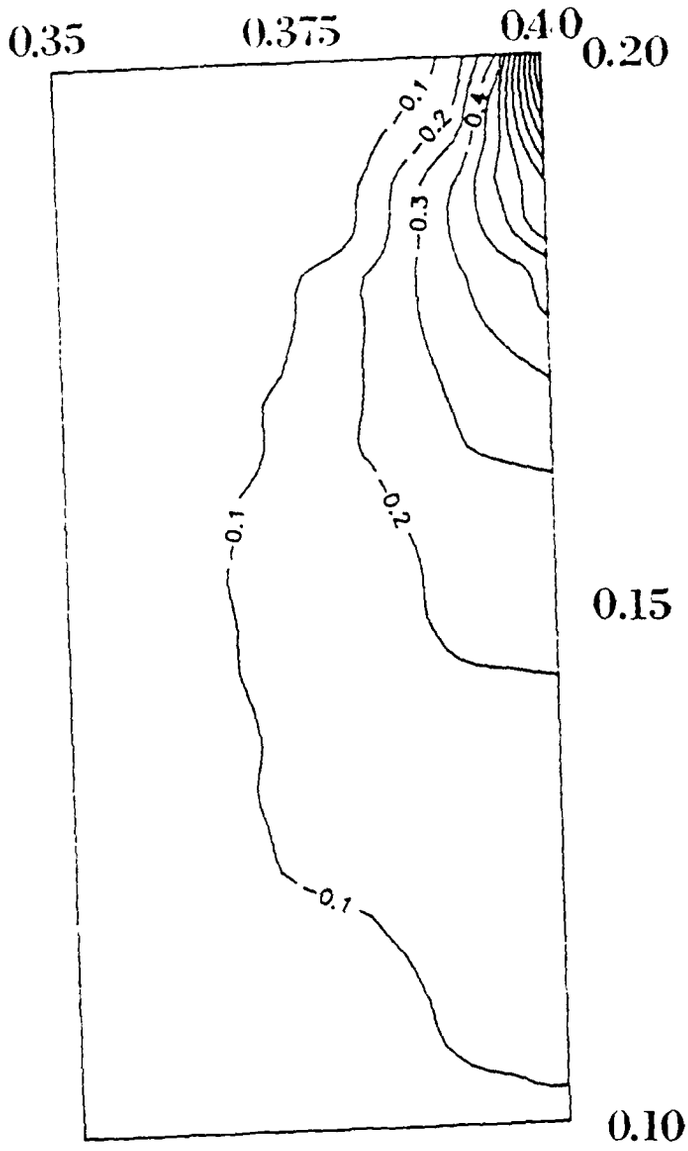

Normal Stress, 95% Stiffness Reduction

Constant Load, P = 3 lb

Fig. 20

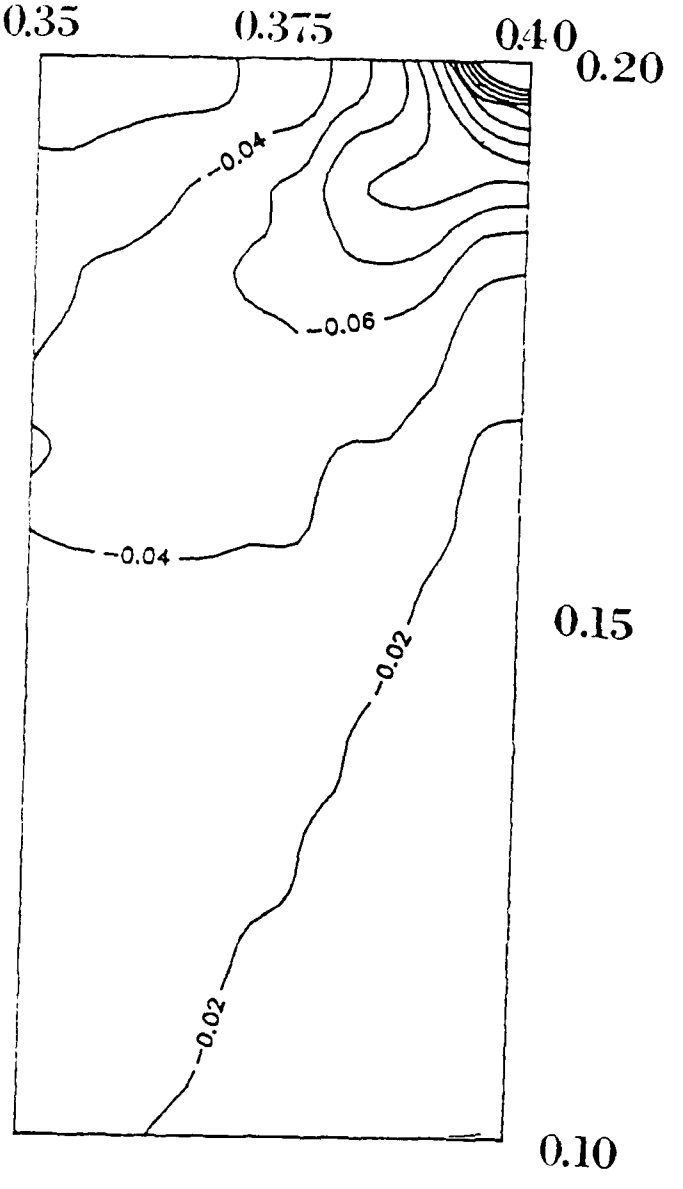

Shear Stress, 0% Stiffness Reduction

Constant Load, P = 3 lb

Fig. 21

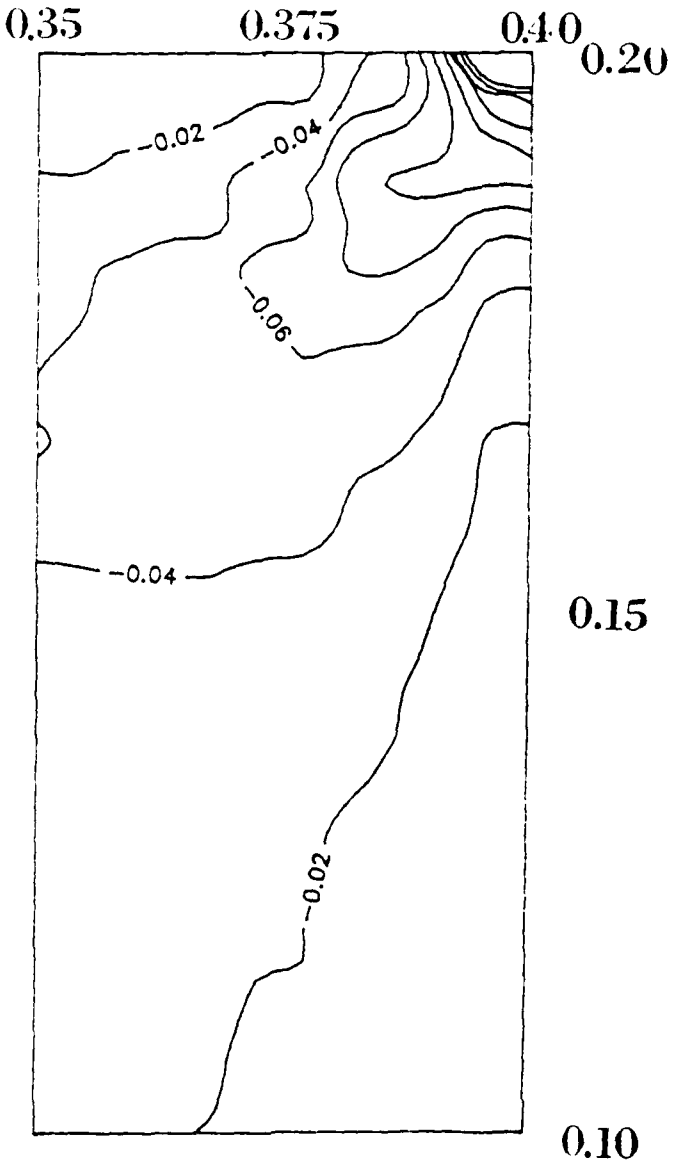

Shear Stress, 50% Stiffness Reduction

Constant Load, P = 3 lb

Fig. 22

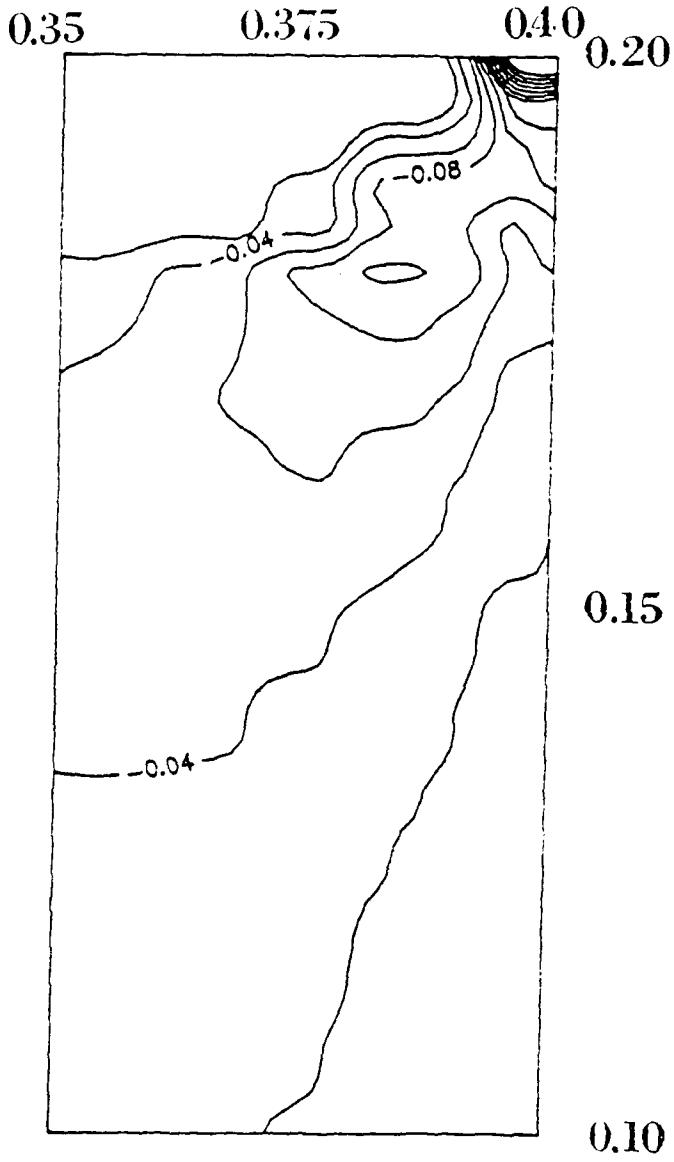

Shear Stress, 95% Stiffness Reduction

Constant Load, P = 3 lb

Fig. 23

along the centerline, but the observed failure path seems to originate close to the load and run to the centerline. The diagonal path taken is similar to that shown by these shear stress contours.

The biggest differences caused by the stiffness reduction technique occurs in the bending stresses. Figure 24 shows the contours resulting from the original single element damage. The reduced stiffness cases are the same when looking away from the damaged element. However, stiffness reduction changes the bending stresses locally. The fifty percent case (Figure 25) shows the compression lines moving toward the load on top of the beam while moving away from the load through the beam's thickness. As the stiffness is reduced to five percent (Figure 26), the point of maximum compression shifts away from the surface to an area under the damaged element. The reduced stiffness element seems to relieve some compression while shifting the load down. This dramatic change in bending stress patterns is not too surprising. The zero degree case shown has the highest modulus along the axis of bending. Reduction causes a larger difference in modulus along this axis than for the normal or shear cases. This big modulus difference then changes the distribution of bending stresses as shown. Although reduced

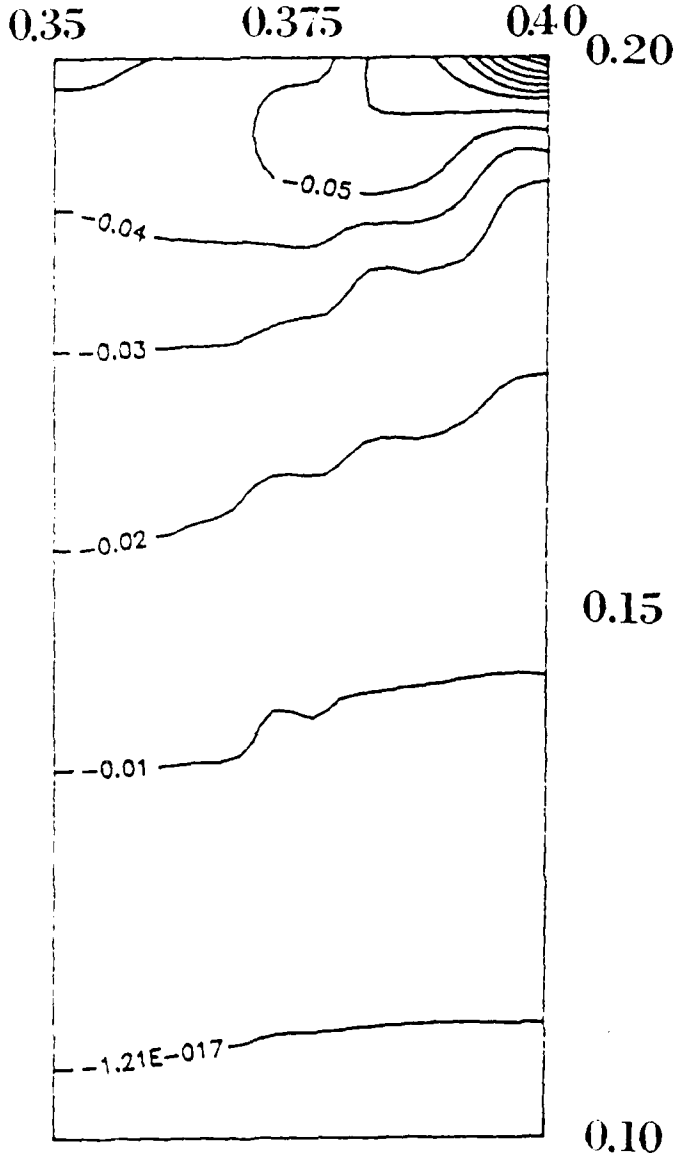

Bending Stress, 0% Stiffness Reduction

Constant Load, P = 3 lb

Fig. 24

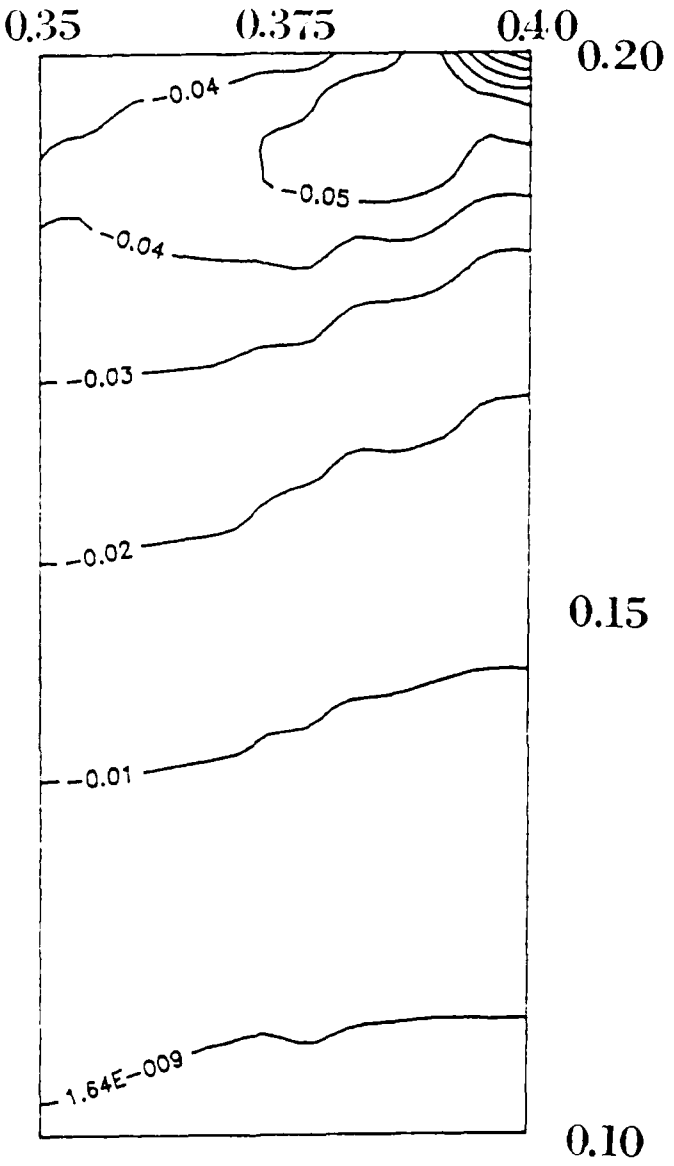

Bending Stress, 50% Stiffness Reduction

Constant Load, P = 3 lb

Fig. 25

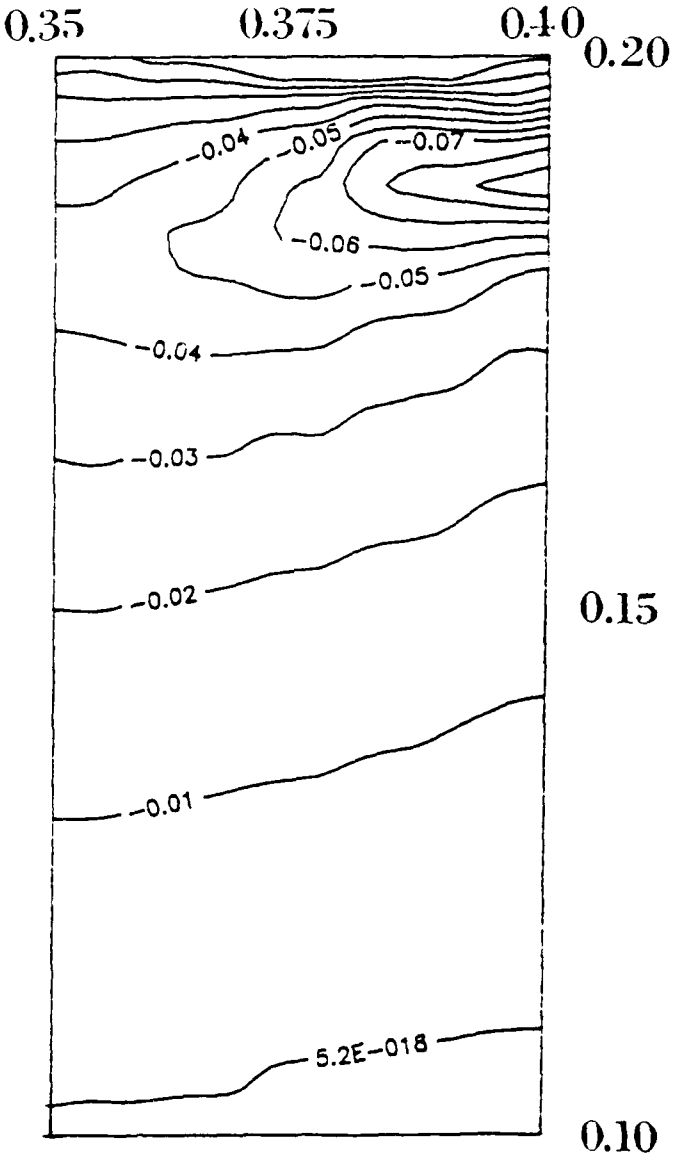

Bending Stress, 95% Stiffness Reduction

Constant Load, P = 3 lb

Fig. 26

the same percentage, the differences in the other material property values are not as great. So normal and shear stresses do not change as dramatically. Since the failure is dominated by normal and shear, the Tsai-Hill plots would not change dramatically with reduction.

The next limiting case tried with a zero degree fiber orientation was to increase the load while holding the damaged element reduction constant at five percent of the original value. The load was a ramp increase from five to twenty pounds in four steps. The program ran for only two steps and stopped with a numerical instability. By the end of the second step, displacements in the failed element were very large. Also, during the third step a non-positive definite stiffness matrix was formed causing program termination. The bending stress (Figure 27) is similar to the constant load case previously discussed. The normal (Figure 28) and shear (Figure 29) stresses show maximums shifting from the surface into the beam. The normal stress shows a zone of highest compression inside the beam. Physically this seems unreasonable as an area of tension cannot exist directly under a compressive load. The damaged area seems to possess an unloading action resulting from the element stiffness

reduction. This is seen as the maximum compression appears to move into the beam. The shear also goes from negative to positive with the high load. This is due to the high stress gradients and the model not having enough detail to pick up all the behavior locally. The continuation of loading with stiffness reduction activated appears to result in the load moving through the beam. However,the reversal in expected stresses, i.e. tension instead of compression, causes this stiffness reduction technique to be suspect.

Ninety Degree Fiber Orientation. Along with the zero degree case, a ninety degree case was run to consider the "isotropic" behavior. The load was held constant while stiffnesses were reduced. Unlike the zero degree case, reductions through five percent of the original stiffness caused no noticeable changes in damage or stress contours. The high modulus axis was along a direction not studied. The axes of interest had moduli of similar low values. Apparently, even a high percentage of reduction did not separate the material properties significantly to change stresses or displacements. The constant load was increased to levels far higher than the initial failure levels with no apparent changes due to stiffness reductions. With no changes in the constant load case, an increasing load with constant reduction case was not attempted.

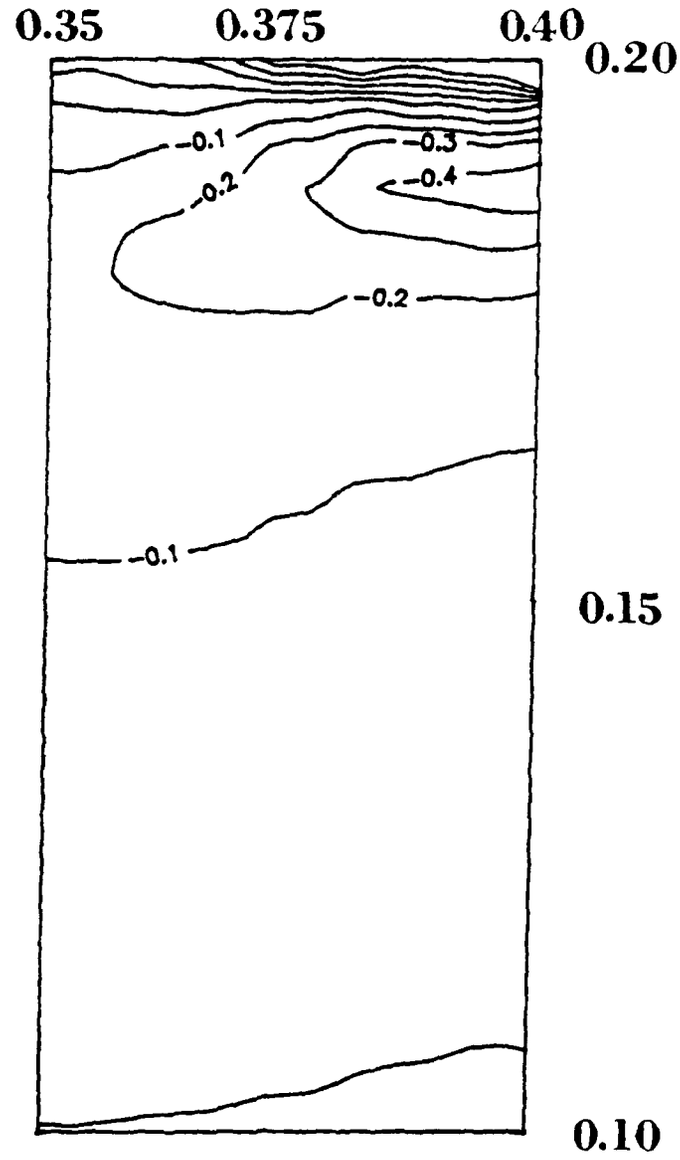

Bending Stress, 95% Stiffness Reduction

Ramp Load

Fig. 27

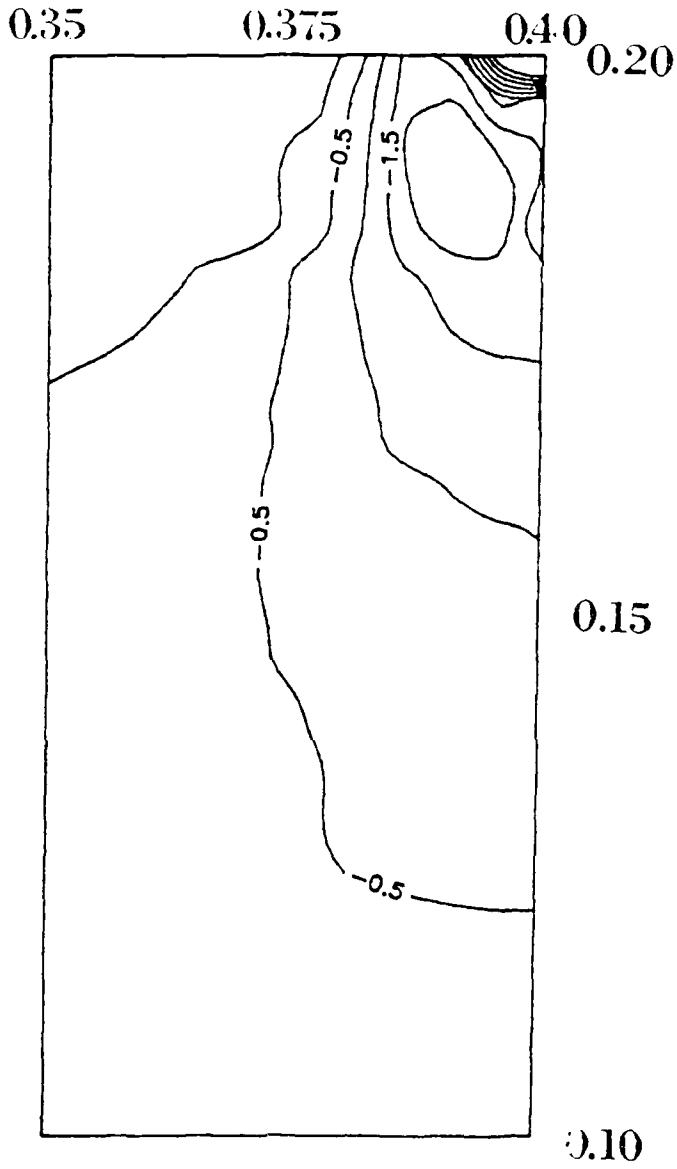

Normal Stress, 95% Stiffness Reduction

Ramp Load

Fig. 28

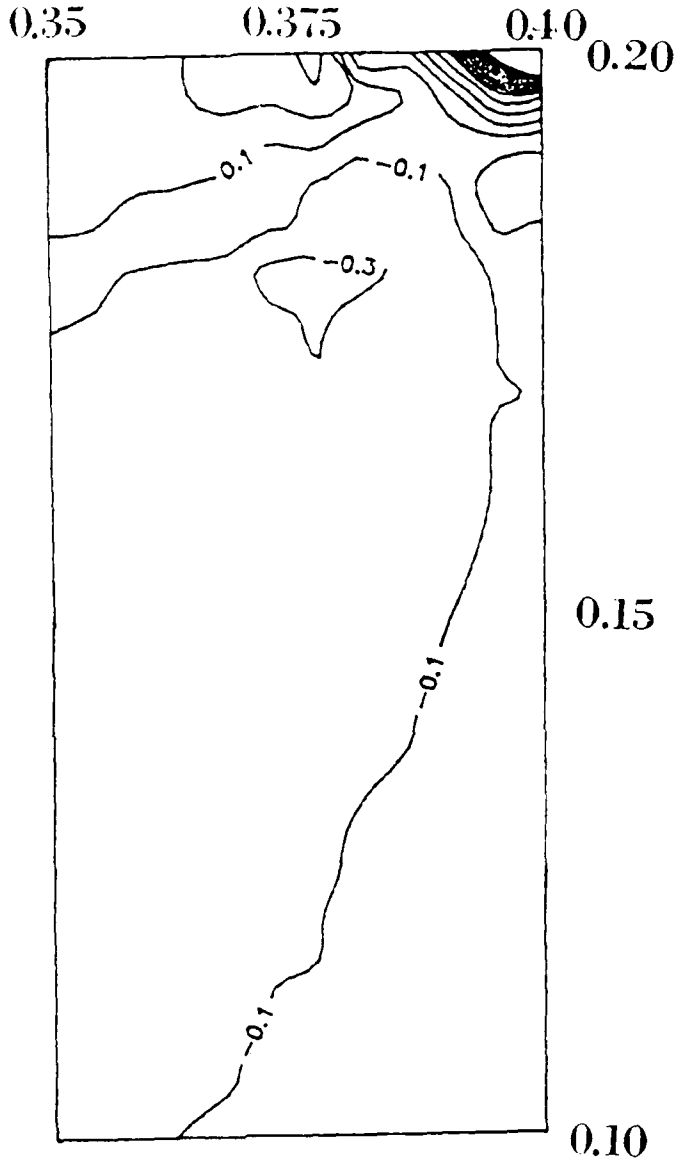

Shear Stress, 95% Stiffness Reduction

Ramp Load

Fig. 29

V. Conclusions and Recommendations

The short beam shear test in composite materials was studied with finite elements to determine a means of modeling damage initiation. The finite element routine used was NOSAPM, a modified version of NONSAP. The complex stress fields associated with this shear test were generated sufficiently around the area of the load application. A subroutine to apply a damage criteria was incorporated into NOSAPM to determine element "failure" in the complex stress field. Also, a stiffness reduction technique was applied where the entire failed element was softened by varying degrees. The results of this study indicate the following:

(1) The convergence study revealed that normal and bending stresses can be obtained fairly well, while shear stress is a function of the mesh size.

(2) The Tsai-Hill failure criteria seems to be readily adaptable to the finite element method.

(3) Fibers oriented ninety degrees appear to be unaffected by the stiffness reduction technique especially with the low modulus properties used.

(4) For zero degree fiber orientation, reductions up to fifty percent result in no drastic changes in failure or stress contours.

(5) Reductions between fifty and ninety-five percent for zero degree fibers show more damage for a constant load.

(6) Stiffness reductions above 95% for the zero degree fiber case showed the originally failed element no longer exceeded the failure criteria, while the load was carried by the adjacent elements.

(7) Increasing the load with ninety-five percent stiffness reduction in zero degree fiber orientation cases does not change the pattern of failures and stress contours except to move the maximums into the body and away from the surface being loaded.

To further this study of damage initiation, one should determine the exact failure modes occurring and then reduce the stiffness in only that part of the element. For example, if the mode of failure was bending, only the modulus along the bending plane would be reduced. Load shifting techniques should also be studied to circumvent program termination due to non-positive stiffness matrix formulations on ill-conditioned elements. Finally, by putting a model of the indenter into the analysis one could avoid the severe point load gradients produced in the single element case.

Appendix A: Using NOSAPM for Stiffness Reduction

The NOSAPM Users Manual (15) describes in detail the use of this finite element code. Modifications were necessary to incorporate the DAMAGE subroutine outlined in Appendix B and the post-processing graphics program SURFER (14). This section deals with three classes of modifications: (1) the input files for NOSAPM, (2) the job control listing (JCL) for the Wright-Patterson AFB (WPAFB) CYBER computer, and (3) the output data files for SURFER. Discussions will include the steps to running both the main program and the associated post-processing.

Preparing Input Files

The NOSAPM input data cards are clearly explained in the users manual (15:1-87). The instructions given should be followed exactly except as indicated in Figure 30. Note that changes and specific values needed to run the stiffness reduction cases are underlined. Also, any cards not shown in the figure can be assumed to be the same as described in the users manual. As can be seen, changing the code to get the necessary formatted data to SURFER restricted NOSAPM to

```
  14   11
 TEST MESH FOR ELEMENT VERIFICATION
  360100111   0    1    1    4    10.000       0.00    1    0
0     0   1
     .
     .
     .
      1    1    1    0    0
      1    1    1    0    0    0    0    1    1    1
      1    4    1
      1    4    1
      1    4    1
      1  180    1
      1    4    1
      1    4    1
      1    1    0    0    1    1    1       0.1      ...
     .
     .
     .
    360    1    1    0    1    1    1       0.0      ...
```

Changes to NOSAPM Data

Fig. 30a

```
      2     1    12     0     0     0     0
      0     0
    3 154    2    0    0    0    0    0    0    2    2    0    0    0    2
4   ...
      1        0.06     3
      8.00E6       1.7E6       1.7E6        0.30        0.02    ...
      .
      .
      .
      4        0.06     3
      3.20E6      0.68E6      0.68E6        0.30        0.02    ...
      76.2E3      79.1E3      13.7E3
      1.0E-3      1.0E-3      1.0E-3
       6.8E3      33.0E3      13.7E3
      1.0E-3      1.0E-3      1.0E-3
       6.8E3      33.0E3      13.7E3
      1.0E-3      1.0E-3      1.0E-3
```

Changes to NOSAPM Data

Fig. 30b

```
  1     8     8     1     1     0     0     1          0.0
 16   196   181     1    17   197   182     2
  0     0     0     0     0     0     0     0     0     0     ...
  .
  .
  .
154     8     8     1     1     0     0     1          0.0
179   359   344   164   180   360   345   165
  0     0     0     0     0     0     0     0     0     0     ...
  1     2     2
      0.00        3.50        40.0        3.50
166     3     1        -1.0         0.0     0
346     3     1        -1.0         0.0     0
STOP
```

Changes to NOSAPM Data

Fig. 30c

the use of rectangular matrices of three dimensional elements using a "2X2" Gaussian integration order. By using another post-processing technique in plotting stresses (or strains) one could eliminate these restrictions.

Running NOSAPM at Wright-Patterson AFB

For this study, NOSAPM was run on the CYBER computer at WPAFB. The length of this program requires that it be run as a batch job using control cards or a JCL. An example of a typical JCL for this study is shown in Figure 31. The steps used for this study are as follows. After initiating the batch job, certain direct access files are opened for processing. The file titled "NOSRUN" is the compiled version of NOSAPM. The three other input files, TAPE91, TAPE31, and TAPE30, are used within NOSAPM to store SURFER formatted data. TAPE91 contains the bending, normal, and shear stresses matched to their corresponding integration points on the face of the beam. These stresses are normalized to the material's compressive strength values. TAPE31 lists the failure criteria values at each integration point on the front face of the beam. TAPE30 shows the elements

```
JWFAK,T2000.
USER,P870075,DUPOQE1.
CHARGE,*.
GET,TAPE5=FNM0SM.
ATTACH,NOSRUN.
DEFINE,TAPE91.
DEFINE,TAPE30.
DEFINE,TAPE31.
NOSRUN,PL=80000.
RETURN,TAPE30.
RETURN,TAPE31.
RETURN,TAPE91.
RETURN,NOSRUN.
#EOR
#EOI
```

Job Control Listing for NOSAPM

Fig. 31

which have exceeded the failure criteria and the integration point(s) in the element where the criteria was exceeded. It is important to remember that in using this JCL one should not already have files TAPE91, TAPE31, and TAPE30 in permanent storage. The JCL creates these files before each run. These output files (TAPE91, TAPE31, and TAPE30) must then be removed or renamed prior to subsequent runs.

Using SURFER for Contour Plotting

With the output files from NOSAPM, contour plotting of stresses and failure criteria are possible. The graphics package used was SURFER, a personal computer resident plotting program. The NOSAPM output files had to be downloaded to a floppy disk using a communications package with an acceptable protocol. The CYBER had XMODEM protocol available for this transfer of files from the mainframe computer to a personal computer. Each NOSAPM generated file usually contained more than one time step. So, the entire listing for each time step had to be separated when placed on the floppy disk. SURFER does accept the ASCII character format resulting from this file transfer.

Actual contouring of the data is best described by the SURFER users manual (14). Note that NOSAPM generates the

data for the entire beam. Since only a small part of the beam is important in this study, much of the NOSAPM data was truncated prior to contouring. This truncation saved processing time and allowed for a more exact contour. The contours are easily viewed with SURFER and displayed by the computer screen, a printer, or a plotter.

Appendix B: Subroutine DAMAGE

The purpose of subroutine DAMAGE was to incorporate failure criteria into the program NOSAPM. It is called during the stress calculation portion of the subroutine THDFE. After the stresses are calculated for each element at the integration points, THDFE calls DAMAGE to compare the stresses against a predetermined failure criteria. So, DAMAGE combines the stress fields generated at each integration point for comparisons against strength criteria. The subroutine is listed in Figures 32a & 32b.

Input to DAMAGE is through common statements. The control character for failure and stiffness reduction is IFAIL(N) where N is the element number. The yield stress and maximum strain are denoted by SSFAIL and SNFAIL, respectively. The control character IFCRIT tells the routine which failure theory to use. Currently DAMAGE only includes the Tsai-Hill criteria. Different theories such as maximum stress and maximum strain can easily be added to DAMAGE. Other input to the subroutine are the stresses or strains of the element. These are calculated at each integration point of the element with another routine in NOSAPM and enter through the common statement MTMD3D.

For the Tsai-Hill theory listed, the code follows the

equations outlined by Jones (8). DAMAGE computes failure using stresses and strengths in combinations determined by the Tsai-Hill relationships. These combinations within DAMAGE result the dimensionless parameter (FTSAI) which if greater than one (1) indicates exceedance of the criteria. For the Tsai-Hill case, ETSAI is the actual dimensionless value of the stress combinations. FTSAI is the check value and is equal to ETSAI minus one (1).

Another calculation performed by DAMAGE is to check the stiffness reduction control character IFAIL(N). At the start of NOSAPM, IFAIL(N) is set to zero (0) for each element. Upon failure of the element, IFAIL(N) becomes one (1). IFAIL(N) increments by one (1) with each succeeding step of the program. With this method, the element(s) failing on earlier time steps would have a higher IFAIL(N) value than those elements just failing. In NOSAPM IFAIL(N) denotes the material property set number for the element. The material property set dictates the state of elemental failure as mentioned in Appendix A.

The output of this subroutine is tailored to the program SURFER. ETSAI is stored to create contour plots of the Tsai-Hill values. The raw data collected here is combined in the main program with the position coordinates of the respective integration point to complete the package for

SURFER. Another piece of the output set up for this study is the listing of the failed elements and the integration points where failure occurred. Thus one can get a quick and easily plotted picture of damage as it progresses not only through the integration points of the element but also through the entire model.

```
      SUBROUTINE DAMAGE
C
C
C     SUBROUTINE TO CHECK FOR FAILURE IN AN ORTHOTROPIC
MATL
C
C     IFCRIT = 0  NO FAILURE CRITERIA
C            = 1  MAXIMUM STRESS USED
C            = 2  MAXIMUM STRAIN
C            = 3  TSAI-HILL THEORY
C
C
      COMMOM/FAIL/IFAIL(300),SSFAIL(3,3),SNFAIL(3,3),IFCRIT
      COMMON/MTMD3D/D(6,6),STRESS(6),STRAIN(6),IPT,N
C
C
      IF(IFCRIT.EQ.1) GO TO 100
      IF(IFCRIT.EQ.2) GO TO 200
      IF(IFCRIT.EQ.0) RETURN
C
C
      CL = 1.0 / (SSFAIL(3,3)**2)
      CM = 1.0 / (SSFAIL(2,3)**2)
      CN = 1.0 / (SSFAIL(1,3)**2)
      CA = 1.0 / (SSFAIL(1,1)**2)
      CB = 1.0 / (SSFAIL(2,1)**2)
      CC = 1.0 / (SSFAIL(3,1)**2)
      CD = CA+CB-CC
      CE = CA+CC-CB
      CF = CC+CB-CA
      FTSAI =CA*(STRESS(1)**2) +CB*(STRESS(2)**2) +
     &        CC*(STRESS(3)**2) -CD*STRESS(1)*STRESS(2) -
     &     CE*STRESS(1)*STRESS(3)-CF*STRESS(2)*STRESS(3)+
     &        CL*(STRESS(6)**2) + CM*(STRESS(4)**2) +
     &        CN*(STRESS(5)**2) - 1.0
      ETSAI = FTSAI + 1.0
      IF(IPT.EQ.5) WRITE(96,4000) ETSAI
      IF(IPT.EQ.6) WRITE(96,4000) ETSAI
      IF(IPT.EQ.7) WRITE(96,4000) ETSAI
      IF(IPT.EQ.8) WRITE(96,4000) ETSAI
 4000  FORMAT(F12.5)
      IF(FTSAI.GT.0.0) GO TO 300
      RETURN
```

Fig. 32a: Source Listing of Subroutine DAMAGE

AD-A194 880 DAMAGE INITIATION IN THE SHORT BEAM SHEAR TEST OF COMPOSITE MATERIALS USI (U) AIR FORCE INST OF TECH WRIGHT-PATTERSON AFB OH SCHOOL OF ENGI D T DUPONT

2/2

UNCLASSIFIED JUN 88 AFIT/GAE/AA/87D-5 F/G 11/4 NL

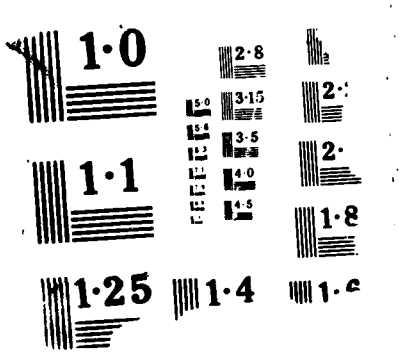
1·0
1·1
1·25
1·4
2·8
3·15
3·5
4·0
4·5
2·
1·8

```
C
C
 100 RETURN
C
C
 200 RETURN
C
C
 300 IF(IFAIL(N).EQ.0) IFAIL(N) = 1
     IF(IPT.LT.8) GO TO 301
     IF(IFAIL(N).GT.0) IFAIL(N) = IFAIL(N) + 1
 301 WRITE(30,1000) N,IPT
 1000FORMAT(8X,16H ELEMENT FAILED ,I4,20H INTEGRATION
POINT  ,I4)
     RETURN
     END
```

Fig. 32: Source Listing of Subroutine DAMAGE

Bibliography

1. American Society for Testing and Materials 1985 Annual Book of ASTM Standards, Section 15, Volume 15.03. Philadelphia, PA. (pp 55-58).

2. Chamis, Christos C., Composite Mechanics for Engine Structures, unpublished report presented at the ASME 1987 Gas Turbine Conference, 31 May - 5 Jun 1987, Anaheim, CA.

3. Chamis, Christos C. and George C. Williams. "Interply Layer Degradation Effects on Composite Structural Response," NASA Technical Memorandum 83702 (May 1984).

4. Cook, Robert D. Concepts and Applications of Finite Element Analysis (Second Edition). New York: John Wiley & Sons, 1981.

5. Copp, Paul D. and Leon M. Keer Smooth Contact of a Rigid Indenter and a Beam of Two Orthotropic Layers. PhD dissertation. Northwestern University, Evanston, Il. December 1986.

6. Hill, R. The Mathematical Theory of Plasticity. Oxford University Press, London, 1950.

7. Humphreys, E. A., Development of an Analytical Procedure to Calculate Damage Accumulation in Composites During Low Velocity Impact: Technical Final Report, July 1981,Contract NAS1-15888/RC, NASA Langley Research Center, Hampton, VA, J1 1981.

8. Jones, Robert M. Mechanics of Composite Materials. New York: Hemisphere Publishing Corporation, 1985

9. Murthy, P.L.N and C.C. Chamis. "Dynamic Stress Analysis of Smooth and Notched Fiber Composite Flexural Specimens," NASA Technical Memorandum 83694 (April 1984).

10. Polakowski N.H and E.J. Ripling, Strength and Structure of Engineering Materials. Prentice-Hall, Inc, Englewood Cliffs, New Jersey, 1966.

11. Ross, C.A., L. E. Malvern and E. L. Jerome, "Modeling of Interlaminar Delamination Using A Finite Element Method," Grant No. DAAG 29-83-K-0107, US Army Research Office, Durham, NC.

12. Shivakumar, K. N. and W. Elber, "Delamination Growth Analysis in Quasi-Isotropic Laminates Under Loads Simulating Low-Velocity Impact," NASA Technical Memorandum 85819, Nasa, Langley Research Center, Hampton VA, June 1984.

13. Shivakumar, K. N., W. Elber and W. Illg, "Analysis of Progressive Damage in Thin Circular Laminates Due to Static-Equivalent Impact Loads," Proceedings 24th AIAA/ASME/ASCE,AHS Structures, Structural Dynamics, and Materials Conference, May 1983.

14. SURFER Users Manual, Golden Software, Golden, CO.

15. Storace, Albert F. Foreign Object Impact Design Criteria-NOSAPM User's Manual. Contract F33615-77-C-5221. Air Force Aero Propulsion Laboratory, Wright-Patterson AFB, January 1985.

16. Storace, Albert F. Foreign Object Impact Design CriteriaU: Final Report September 1977-September 1983. Contract F33615-77-C-5221. Aero Propulsion Lab, Wright-Patterson AFB, January 1985 (AFAPL-TR-78-81).

17. Tsai, Stephen W. "Strength Theories of Filamentary Structures" in Fundamental Aspects of Fiber Reinforced Plastic Composites, edited by R.T. Schwartz and H.S. Schwartz. New York: Wiley Interscience, 1968, pp3-11.

18. Tsai, Stephen W. and H. Thomas Hahn Introduction to Composite Materials. Westport: Technomic Publishing Company, 1980.

19. Tsai, Stephen W. and Edward M. Wu, "A General Theory of Strength for Anisotropic Materials," Journal of Composite Materials, 5: 58-80 (January 1971).

20. Whitney, J. M. and C. E. Browming, "On Short Beam Shear Tests for Composite Materials," Experimental Mechanics, 25: 294-300 (1985).

21. Witt, Capt William P. A Numerical Analysis of Fracture in a Laminated Fibrous Composite Plate. MS thesis, AFIT/GA/AA/77D-9. School of Engineering, Air Force Institute of Technology (AU), Wright-Patterson AFB OH, December 1977.

22. Wu, Edward M. "Phenomenological Anisotropic Failure Criterion," Composite Materials: Volume 2 Mechanics of Composite Materials. 353-431. Academic Press, New York, 1974.

VITA

Captain D. Thomas Dupont was born on 15 August 1960 in Moses Lake, Washington. He graduated from high school in Summerville, South Carolina, in 1978 and attended Clemson University, from which he received the degree of Bachelor of Science in Mechanical Engineering in May 1982. Upon graduation, he received a commission in the USAF through the ROTC program. His first assignment was as a program manager at the Ballistic Missile Office, Norton AFB, CA, until February 1986. He then attended Squadron Officers School in Maxwell AFB, AL, before entering the School of Engineering, Air Force Institute of Technology, in June 1986.

Permanent address: 2902 Stratford Ct.
Arlington, Texas 76015

REPORT DOCUMENTATION PAGE

Form Approved
OMB No. 0704-0188

1a REPORT SECURITY CLASSIFICATION UNCLASSIFIED	1b. RESTRICTIVE MARKINGS
2a SECURITY CLASSIFICATION AUTHORITY	3. DISTRIBUTION/AVAILABILITY OF REPORT Approved for public release, distribution unlimited.
2b. DECLASSIFICATION/DOWNGRADING SCHEDULE	
4 PERFORMING ORGANIZATION REPORT NUMBER(S) AFIT/GAE/AA/87D-5	5. MONITORING ORGANIZATION REPORT NUMBER(S)
6a NAME OF PERFORMING ORGANIZATION School of Engineering 6b. OFFICE SYMBOL (*If applicable*) AFIT/ENY	7a. NAME OF MONITORING ORGANIZATION
6c. ADDRESS (*City, State, and ZIP Code*) Air Force Institute of Technology Wright-Patterson AFB OH 45433- 6583	7b. ADDRESS (*City, State, and ZIP Code*)
8a. NAME OF FUNDING/SPONSORING ORGANIZATION 8b. OFFICE SYMBOL (*If applicable*)	9. PROCUREMENT INSTRUMENT IDENTIFICATION NUMBER
8c. ADDRESS (*City, State, and ZIP Code*)	10. SOURCE OF FUNDING NUMBERS PROGRAM ELEMENT NO. / PROJECT NO. / TASK NO / WORK UNIT ACCESSION NO.
11. TITLE (*Include Security Classification*) See Box 19	
12. PERSONAL AUTHOR(S) D. Thomas Dupont, B.S., Capt, USAF	
13a. TYPE OF REPORT MS Thesis 13b. TIME COVERED FROM _____ TO _____	14. DATE OF REPORT (*Year, Month, Day*) 1988 June 15. PAGE COUNT 92
16. SUPPLEMENTARY NOTATION	

17. COSATI CODES		
FIELD	GROUP	SUB-GROUP
11	04	

18. SUBJECT TERMS (*Continue on reverse if necessary and identify by block number*)
Composite Materials, Shear Test, Stiffness Reduction, Damage Initiation, Finite Elements

19. ABSTRACT (*Continue on reverse if necessary and identify by block number*)

Title: DAMAGE INITIATION IN THE SHORT BEAM SHEAR TEST OF COMPOSITE MATERIALS

Thesis Chairman: Paul D. Copp, Major, USAF
Associate Professor of Aeronautical Engineering

Approved for public release: IAW AFR 190-1.
LYNN E. WOLAVER 15 Jun 88
Dean for Research and Professional Development
Air Force Institute of Technology (AU)
Wright-Patterson AFB OH 45433

20. DISTRIBUTION/AVAILABILITY OF ABSTRACT ☒ UNCLASSIFIED/UNLIMITED ☐ SAME AS RPT ☐ DTIC USERS	21 ABSTRACT SECURITY CLASSIFICATION UNCLASSIFIED
22a NAME OF RESPONSIBLE INDIVIDUAL Paul D. Copp, Major, USAF	22b TELEPHONE (*Include Area Code*) (513) 255-2632 22c OFFICE SYMBOL AFIT/ENY

DD Form 1473, JUN 86 *Previous editions are obsolete*

The purpose of this study was to analyze damage initiation in the short beam shear test for composite materials. This thesis proposes a means of predicting damage initiation in a composite beam using finite element techniques and a continuum mechanics failure criteria. The first objective was to accurately determine the stress field. The second objective was to employ a damage criteria based on the elemental stress field. The final objective was to evaluate the effectiveness of using an elemental stiffness reduction to study damage initiation and progression. The finite element code used was NOSAPM.

The complex stress fields associated with this problem were accurately obtained with the exception of the shear stresses. The high shear gradients required the use of a very fine mesh which was not possible with the computer resources available. The Tsai-Hill failure criteria was successfully incorporated into NOSAPM. Also, an elemental stiffness routine was derived and verified with a single element compression case. With the beam test model, the stiffness reduction technique did not dramatically affect the material with fibers oriented ninety degrees. However, the zero degree fiber orientation case resulted in stress contour changes which suggested a spreading of the load through an element. This spreading only occurred with a stiffness reduction greater than ninety-five percent. At high loads and stiffness reductions, the model breaks down as the numerical solutions result in element instabilities.

END
DATED
FILM
8-88
DTIC